Prospects for Probing the Three Gauge-boson Couplings in $W + Z$ Production at the LHC

Matt Dobbs* and Michel Lefebvre†

Department of Physics and Astronomy, University of Victoria, P.O. Box 3055, Victoria, British Columbia, Canada V8W 3P6

(Dated: September 16, 2002)

We assess the prospects for directly probing the WWZ triple gauge-boson coupling by means of hadronic WZ production at the 14 TeV Large Hadron Collider (LHC) using the ATLAS detector. We compare the sensitivity to anomalous couplings of different analysis techniques, including a new application for hadron colliders of the "Optimal Observables" analysis strategy. We account for the effects of higher order QCD corrections and the contributions to the sensitivity from other theoretical and detector related systematic effects.

ATL-PHYS-2002-023
08/10/2002

Contents

I. Introduction 2

II. Phenomenology 2

III. Detector and Physics Simulation 5

IV. Backgrounds and Event Selection 6
A. Backgrounds with a Tri-lepton Signature 7
B. Jets Mis-Identified as Electrons 7
C. Event Selection and Efficiency 8

V. Analysis Methods and Results 9
A. Measuring Anomalous Coupling Parameters and Evaluating Systematics 10
B. Optimal Observables 16
C. Results and Comparison of Methods 20
D. Limits as a Function of Integrated Luminosity 24
E. Limits as a Function of Form Factor Scale and Mass Scale 25

VI. Conclusions 27

Acknowledgements 28

References 28

Appendix 30
Effect of Isolation Criteria on $Z \to e^+e^-$ Decays 30

*Electronic address: matt.dobbs@cern.ch
†Electronic address: lefebvre@uvic.ca

I. INTRODUCTION

In the Standard Model (SM), the gauge structure of the WWZ triple gauge-boson coupling (TGC) produces cancellations in the production of W^+W^- and $W^\pm Z$ pairs. Without these cancellations, the cross section for longitudinally polarised W^+W^- and $W^\pm Z$ pairs would grow proportional to the diboson invariant mass squared, violating unitarity at relatively low energies. Because these cancellations are so important for the consistency of the model, it is necessary to test them at the highest accuracy possible. While the $pp \to W^+W^-$ mechanism receives contributions from both the WWZ and $WW\gamma$ coupling, the $pp \to W^\pm Z$ channel allows for the direct independent measurement of the WWZ coupling. Similarly, the $pp \to W^\pm\gamma$ channel can be used to independently measure the $WW\gamma$ coupling.

This paper focuses on the prospects of measuring anomalous contributions to the WWZ coupling through $pp \to W^\pm Z \to l^\pm\nu l^+l^-$ production (where l is an electron or muon) at the LHC with the ATLAS detector. The analysis is optimised for so-called "low luminosity" ($10^{33}\mathrm{cm}^{-2}\mathrm{s}^{-1}$) LHC conditions. This study complements the analysis of $W\gamma$ production which has been presented in Ref. [1]. Many of the considerations discussed in that paper are relevant for the WZ channel, and we refer the reader to the discussions presented there. The WZ channel has previously been studied in the context of ATLAS in Refs.[2, 3]. This paper extends those analyses by exploring new analysis techniques, performing the simulations at NLO, and evaluating systematic effects. For a study of the charged neutral TGC couplings in ZZ and $Z\gamma$ production, see Refs. [4]. The $pp \to W^+W^-$ channel has not been studied by the ATLAS collaboration thus far.

The structure of this paper is as follows. Phenomenology relevant to the WWZ couplings is discussed in the next section. The software chain which has been used to simulate the physics processes and detector are reviewed in Section III. Backgrounds and the kinematic cuts which are used to isolate the signal are presented in Section IV. Several methods for measuring the TGC vertex are described, evaluated, and compared in Section V before summarising the study in the concluding section.

II. PHENOMENOLOGY

The most general Lorentz and gauge invariant anomalous WWZ TGC vertex is described by 7 parameters (ignoring any theoretical or experimental constraints) and may be written in terms of an effective Lagrangian [5–7],

$$\begin{aligned} i\mathcal{L}^{WWZ}/g_{WWZ} &= [1+\Delta g_Z^1]V^\mu(W^-_{\mu\nu}W^{+\nu} - W^+_{\mu\nu}W^{-\nu}) \\ &+ [1+\Delta\kappa_Z]W^+_\mu W^-_\nu V^{\mu\nu} \\ &+ \frac{\lambda_Z}{M_W^2}V^{\mu\nu}W^{+\rho}_\nu W^-_{\rho\mu} \\ &+ ig_Z^4 W^-_\mu W^+_\nu(\partial^\mu V^\nu + \partial^\nu V^\mu) \\ &+ ig_Z^5\varepsilon_{\mu\nu\rho\sigma}[(\partial^\rho W^{-\mu})W^{+\nu} - W^{-\mu}(\partial^\rho W^{+\nu})]V^\sigma \\ &- \frac{\tilde\kappa_Z}{2}W^-_\mu W^+_\nu\varepsilon^{\mu\nu\rho\sigma}V_{\rho\sigma} \\ &- \frac{\tilde\lambda_Z}{2M_W^2}W^-_{\rho\mu}W^{+\mu}_\nu\varepsilon^{\nu\rho\alpha\beta}V_{\alpha\beta} \end{aligned} \tag{1}$$

Anomalous Coupling Parameter	Operator Dimensionality	Odd Transformations
Δg_Z^1	4	
$\Delta\kappa_Z$	4	
λ_Z	6	
g_Z^4	4	C, CP
g_Z^5	4	C, P
$\tilde{\kappa}_Z$	4	P, CP
$\tilde{\lambda}_Z$	6	P, CP

TABLE I: The dimensionality and transformation properties of the WWZ anomalous TGC parameters are summarized.

where M_W is the W-boson mass, V^μ and W^μ are the Z and W fields, $W_{\mu\nu} = \partial_\mu W_\nu - \partial_\nu W_\mu$, and $V_{\mu\nu} = \partial_\mu V_\nu - \partial_\nu V_\mu$. The normalisation factor is chosen for convenience to be $g_{WWZ} = -e\cot\theta_W$.

As they are written in Equation 1, all anomalous TGC's are zero in the SM. The operator in the Lagrangian with coefficient g_Z^5 is charge (C) and parity (P) odd. The operators with coefficients g_Z^4, $\tilde{\kappa}_Z$, and $\tilde{\lambda}_Z$ parameterise possible CP violation in the bosonic sector because they are CP odd. The properties of the anomalous TGC's are summarised in Table I. For simplicity, most studies assume separate C and P conservation, which reduces the number of anomalous TGC's for the WWZ vertices to three: Δg_Z^1, $\Delta\kappa_Z$, and λ_Z.

Prior to 1998, the LEP collaborations were using a different parameterisation which combined the WWZ and $WW\gamma$ vertex C and P conserving anomalous parameters (Δg_Z^1, $\Delta\kappa_Z$, λ_Z, $\Delta\kappa_\gamma$, and λ_γ) into just three independent coefficients [8] $\alpha_W, \alpha_{W_\phi}, \alpha_{B_\phi}$. This scenario assumes $\lambda_\gamma = \lambda_Z$ and $\Delta\kappa_Z = \Delta g_Z^1 - \Delta\kappa_\gamma \tan^2\theta_W$. The relationships between these coefficients and the ones presented in Eq. 1 are

$$\begin{aligned} \Delta g_Z^1 &= \frac{\alpha_{W_\phi}}{\cos^2\theta_W} \\ \lambda_\gamma = \lambda_Z &= \alpha_W \\ \Delta\kappa_\gamma &= \alpha_{W_\phi} + \alpha_{B_\phi} \\ \Delta\kappa_Z &= \alpha_{W_\phi} - \frac{\sin^2\theta_W}{\cos^2\theta_W}\alpha_{B_\phi}. \end{aligned} \tag{2}$$

The HISZ scenario [9] has been used by both the CDF and D0 collaborations and further reduces the number of independent coefficients to two by requiring (somewhat arbitrarily) $\alpha_{W_\phi} = \alpha_{B_\phi}$.

If any of the anomalous TGC parameters are introduced into the Lagrangian as constants, unitarity will eventually be violated at energy scale Λ, given by [10]

$$\Lambda^2 = \frac{0.54\ \text{TeV}^2}{|\lambda_Z|}, \qquad \Lambda^2 = \frac{0.85\ \text{TeV}^2}{|\Delta\kappa_Z|}, \qquad \Lambda^2 = \frac{0.87\ \text{TeV}^2}{|\Delta g_Z^1|}. \tag{3}$$

Cancellations may occur if more than one anomalous coupling is allowed non-zero at a time, which weakens these unitarity limits somewhat. We emphasise that in the SM, diboson production satisfies unitarity because of the cancellations between Feynman graphs containing different couplings, and so there is no reason to assume the absence of subtle cancellations between the anomalous TGC parameters which would alter the unitarity limits of Eq. 3.

Nevertheless, to safe-guard unitarity, the most common approach is to introduce the anomalous couplings into the Eq. 1 Lagrangian as energy dependent form factors which go smoothly to zero at high energy scales,

$$\lambda_Z = \frac{\lambda_{Z0}}{(1+\frac{M^2_{\text{W}\gamma}}{\Lambda^2_{\text{FF}}})^n}, \qquad \Delta\kappa_Z = \frac{\Delta\kappa_{Z0}}{(1+\frac{M^2_{\text{W}\gamma}}{\Lambda^2_{\text{FF}}})^n}, \qquad \Delta g_Z^1 = \frac{\Delta g_{Z0}^1}{(1+\frac{M^2_{\text{W}\gamma}}{\Lambda^2_{\text{FF}}})^n}, \tag{4}$$

where $n > 1/2$ is sufficient for the $\Delta\kappa_Z$ coupling and $n > 1$ is sufficient for the λ_Z and Δg_Z^1 couplings. Notice that this means each anomalous coupling is no longer parametrised by a single coefficient, but now has 3 parameters, i.e. the λ_Z anomalous TGC is parametrised by λ_{Z0}, $\Lambda_{\rm FF}$, and n. The usual choice for the WWZ and $WW\gamma$ anomalous couplings is $n = 2$, and $\Lambda_{\rm FF}$ is often chosen so large (e.g. $\Lambda_{\rm FF}$=2 TeV for the Tevatron) that the effects of the form factor are not apparent at the scale at which the experiment probes.

Though the anomalous TGC limits presented in this paper will be given as a function of the dipole form factor scale of Eq. 4 (to allow for comparisons with other analyses), the authors prefer to avoid the unnecessary dependence of experimental limits on the form factor choice by reporting experimental anomalous TGC confidence limits as a function of the diboson invariant mass being probed. To this end, the limits will be reported as a function of a diboson invariant mass cutoff which is applied to the data. As will be discussed in Sec. V, the LHC is sensitive to WZ invariant masses up to about 3 TeV. Using a mass cutoff of 3 TeV or higher (which effectively means no cutoff is applied), will give the best anomalous TGC limits, and represents the maximum reach of the experiment. As the mass cutoff is decreased below 3 TeV, the confidence limits will degrade somewhat. So long as the mass cutoff satisfies Eq. 3, unitarity is ensured without the introduction of extra parameters. Further, if an anomalous coupling 'turns on' or 'turns off' at some mass scale, that would be reflected in the limits.

In order to better understand how the effective Lagrangian relates to kinematic variables, the approximate modifications to the matrix element amplitudes are presented here. In the high energy limit ($\hat{s} >> M_W^2$, where $\sqrt{\hat{s}}$ is the parton centre of mass energy) the change in the matrix element $\Delta\mathcal{M}_{H_Z,H_W}$ arising from anomalous TGC's for the leading order partonic process $q\bar{q}' \to WZ$ are [6],

$$\Delta\mathcal{M}_{\pm,0} \propto \frac{\sqrt{\hat{s}}}{2M_W}[\Delta g_Z^1 + \Delta\kappa_Z + \lambda_Z]\ \frac{1}{2}(1 \mp \cos\theta_Z^\star), \tag{5}$$

$$\Delta\mathcal{M}_{\pm,\pm} \propto \frac{\hat{s}}{2M_W^2}[\lambda_Z]\ \frac{1}{\sqrt{2}}\sin\theta_Z^\star, \tag{6}$$

$$\Delta\mathcal{M}_{0,\pm} \propto \frac{\sqrt{\hat{s}}}{2M_W}[2\Delta g_Z^1 + \lambda_Z]\ \frac{1}{2}(1 \pm \cos\theta_Z^\star), \tag{7}$$

$$\Delta\mathcal{M}_{0,0} \propto \frac{\hat{s}}{2M_W^2}[\Delta g_Z^1]\ \frac{1}{\sqrt{2}}\sin\theta_Z^\star \tag{8}$$

where H_Z, H_W are the Z, W helicities and $\theta_Z^\star$ is the production angle of the Z with respect to the quark direction in the parton centre of mass frame. The effect of C or P odd anomalous TGC's have been omitted and $\frac{\sqrt{\hat{s}}}{2M_W} \approx \frac{\sqrt{\hat{s}}}{2M_Z}$ has been assumed to simplify the equations. Because the Z-boson is a massive particle, $H_Z = 0$ is allowed, and so there are three more possibilities for the helicity amplitudes $(H_Z, H_W) = (0,+),\ (0,-),\ (0,0)$ than for the $pp \to W\gamma$ case.

The importance of the dimensionality of the Lagrangian operators is apparent in Eqs. 5-8. The λ_Z coupling is the coefficient of a dimension six operator, and it enhances the cross section by a factor proportional to the parton centre of mass energy squared $\hat{s}$. The $\Delta\kappa_Z$ parameter is the coefficient of a dimension four operator, and its enhancement is proportional only to $\sqrt{\hat{s}}$. For four of the five amplitudes in which the Δg_Z^1 coupling appears, it is enhanced only by a factor proportional to $\sqrt{\hat{s}}$. For the (0,0) amplitude, however, it receives an enhancement proportional to $\hat{s}$. This, together with the angular dependence, means the sensitivity to the Δg_Z^1 parameter is expected to be better (worse) than for the $\Delta\kappa_Z$ (λ_Z) parameter at a high energy collider such as the LHC.

The effects of anomalous TGC's are largest when the gauge-bosons are centrally produced

at high energy, i.e. when the transverse momentum of the gauge-bosons is large. This is the kinematic region which will provide the best sensitivity to anomalous TGC's. It is also the region where the effects of higher order QCD corrections are most important. Whereas NLO QCD corrections increase the inclusive LHC WZ cross section by only about 30% [11], at high transverse momentum, this enhancement can be as large as a factor 2-10. The NLO corrections are further enhanced in the central production regions, because subtle gauge cancellations at Born level reduce the contributions from the Feynman graphs containing the TGC vertex. These cancellations are referred to as the "radiation zero" [12], and are exact for $W\gamma$ production, and approximate for WZ production [13]. The $\mathcal{O}(\alpha_S)$ diagrams which are responsible for this high transverse momentum enhancement do not contain the TGC vertex, and so the net effect of QCD corrections is a spoiling of the sensitivity to the anomalous TGC's. Though a veto acting on the jet activity within the candidate events is largely effective at reducing the effect of higher order corrections, it is nevertheless important to account for these effects to assess the sensitivity of the ATLAS experiment to the anomalous TGC parameters.

The most stringent direct limits on the anomalous TGC parameters have been achieved by the LEP experiments ALEPH, DELPHI, L3, and OPAL. The results from the four experiments have been combined in Ref. [14], which includes only the data up to the end of 1999 at a centre-of-mass energy up to 202 GeV (i.e. does not yet include all of the data from LEP 2). The LEP combined 95% confidence intervals are

$$\begin{aligned} -0.089 < \lambda_\gamma < 0.20, \\ -0.13 < \Delta\kappa_\gamma < 0.13, \\ -0.074 < \Delta g_Z^1 < 0.028 \end{aligned} \tag{9}$$

assuming the WWZ and $WW\gamma$ vertex anomalous TGC parameters are related by $\lambda_\gamma = \lambda_Z$ and $\Delta\kappa_Z = \Delta g_Z^1 - \Delta\kappa_\gamma \tan^2\theta_W$.

III. DETECTOR AND PHYSICS SIMULATION

The signal, backgrounds, and detector have been simulated in exactly the same manner as discussed in Ref. [1] for $pp \to W\gamma$. The software chain is shown in Figure 1.

The $pp \to W^\pm Z \to l^\pm \nu l^+ l^-$ signal events have been generated at NLO in QCD with the Baur, Han, and Ohnemus (BHO) generator [11] using the CTEQ4M [15] structure functions. The BHO generator has been modified to provide the event weights as a function of the anomalous coupling parameters, as discussed in the appendix of Ref.[1]. The events produced by the BHO generator contain the leptonic decay products of the gauge-boson, and at most one coloured parton in the final state. For the events with a coloured parton in the final state, the method of *independent fragmentation* is used (see e.g. section 5.6.1 of Ref. [16] for a description), followed by *hadronization*, to produce the colour-singlet particles which form the input to the detector simulation. The `PYTHIA` 6.136 [17] program is used for independent fragmentation and hadronization. The standard parton shower approach cannot be applied to the events produced by the BHO generator, because this would double count regions of phase space.

`PYTHIA` 6.136 has been used for the simulation of the background processes. A single constant k-factor of 1.5 has been applied to all of the background process cross sections to account for the effect NLO corrections will have on the total background rate.

The response of the ATLAS detector to the final state particles is modelled using the ATLAS fast simulation program `ATLfast` [18] version 2.55. A complete description of the ATLAS detector is available in Ref. [19] and references therein. The `ATLfast` program does not include

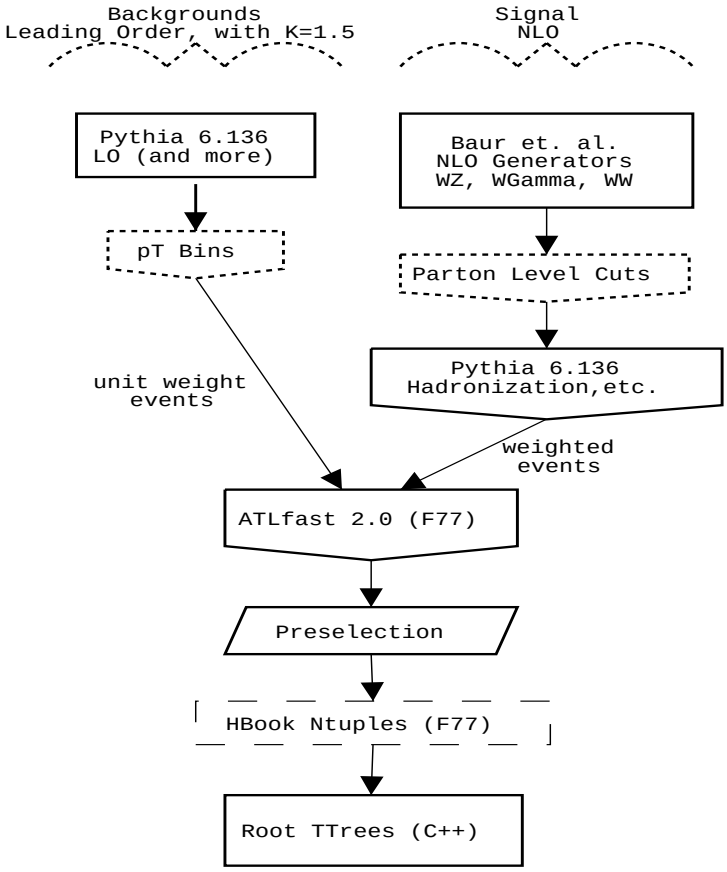

FIG. 1: The event generation chain is shown schematically for the background processes (left branch) and the signals (right branch).

reconstruction efficiencies, or particle mis-identification, and these effects are added "by hand" in the manner described in Ref. [1]. The efficiency for the reconstruction of electrons and muons is taken as 73% and 95%, respectively. The rejection factor [19, 20] against jets faking electrons is taken as 10^5 (i.e. one out of every 10^5 jets will be mis-identified as an electron). The rate of fake high P^T muons will be negligible in ATLAS [21].

The reconstructed electron, muon, and photon candidates are required to satisfy isolation criteria. For this study, the default isolation criteria implemented in the `ATLfast` program have been used. We note that for Z transverse momenta above about 450 GeV, these criteria can substantially degrade the efficiency for reconstructing $Z \to e^+e^-$ decays, because the electron and positron are too collimated in azimuthal angle and pseudorapidity space to survive the isolation cuts. This does not affect the present analysis, because fewer than one event is expected in this transverse momentum regime. We discuss this topic further in the appendix, since it may be relevant for studies of WZ production at high luminosity.

IV. BACKGROUNDS AND EVENT SELECTION

The WWZ vertex will be probed at ATLAS using the process $pp \to W^{\pm}Z \to l^{\pm}\nu l^+l^-$ where l denotes an electron or muon type lepton and ν is a neutrino or antineutrino. Hadronic decay channels are difficult to separate from QCD backgrounds, and the addition of these channels are not expected to significantly improve the precision of the measurements.

This process provides a striking signature in the detector: three high transverse momentum charged leptons, two of which are like-flavor opposite sign and reconstruct to the Z mass, and

large missing transverse momentum ($P^T_{\rm miss}$) arising from the neutrino. Only a few backgrounds mimic this signature.

The ATLAS trigger for these events will be the single muon and single electron triggers, operating at $P^T_\mu = 20$ GeV and $P^T_{\rm e} = 25$ GeV respectively for low luminosity running [19, Table 11-20].[1] At high luminosity, the electron trigger will be further increased to at least $P^T_{\rm e} = 30$ GeV, in this case the $P^T_{\rm e} = 20$ GeV two-electron trigger (which requires the presence of two electrons, each having at least $P^T_{\rm e} = 20$ GeV) can be used in conjunction with the $P^T_\mu = 20$ GeV muon trigger.

In this section, we summarise the processes which contribute to the backgrounds and then present the kinematic cuts which optimise the selection of event candidates.

A. Backgrounds with a Tri-lepton Signature

ZZ with leptonic decays This diboson process will mimic the signature for WZ production when one of the charged leptons from the Z decays escapes detection.

The process is simulated with the PYTHIA 6.136 ZZ process (MSUB(22) switch in PYTHIA) by forcing the Z's to decay to charged leptons. The scenario where one Z decays to electron or muon type leptons and the other one decays to τ's (with one $\tau^\pm \to l^\pm\nu\nu$) provides a difficult signature (three charged leptons and $P^T_{\rm miss}$).

B. Jets Mis-Identified as Electrons

Heavy flavors $t\bar{t}$ Heavy flavors can provide significant backgrounds, particularly $t\bar{t} \to WbW\bar{b}$ with the W's decaying leptonically. The contribution from $b\bar{b}$ is negligible (and has been checked).

This process is simulated with PYTHIA 6.136 (MSEL=5,6 switches in PYTHIA). The simulation with PYTHIA does not account for the $t\bar{t}Z$ final state, which is a potentially dangerous background when the Z decays to charged leptons. The cross section for $pp \to t\bar{t}Z \to 3l^\pm + X$ at 16 TeV has been calculated in Ref. [22] to be about 18 fb (for a top quark mass of 175 GeV) requiring $P^T_{\rm l^\pm}$ >20 GeV and $|\eta_{\rm l^\pm}|$ <2.5 for all of the charged leptons. The slightly lower LHC energy (14 TeV), together with a jet veto and lepton isolation criteria should be sufficient to bring the $t\bar{t}Z$ contribution well below 1 fb, making its contribution very small. The $t\bar{t}Z$ background is neglected in this analysis.

Z+jet production Though the cross section for this process is very large, the rejection factor for jets mis-identified as electrons is also large (10^5). There is no direct source of missing transverse energy for this background, so a $P^T_{\rm miss}$ cut will be effective at reducing its contribution.

PYTHIA 6.136 processes $q\bar{q} \to Zg$ and $g\overset{(-)}{q} \to Z\overset{(-)}{q}$ (MSUB(15),MSUB(30) switches in PYTHIA) with the Z forced to decay to leptons are used to simulate this background.

[1] The $P^T_{\rm e} = 20$ GeV single isolated electron trigger reported in Table 11-20 of Ref. [19] has been increased to a $P^T_{\rm e} = 25$ GeV trigger. A pre-scaled e20i trigger will still be available. If these trigger thresholds are further increased, the WZ analysis will start to be affected—though some of the loss can be recovered by using also the 15 GeV di-electron (2e15i) trigger at low luminosity.

	Z+jet	ZZ	$t\bar{t}$
preselection	631	576	745
3 leptons, $P^T_{\mathrm{l}^\pm} > 25$ GeV	398	500	461
$P^T_{\mathrm{miss}} > 25$ GeV	3.2	90	357
$\lvert M_{\mathrm{l}^+\mathrm{l}^-} - M_{\mathrm{Z}}\rvert < 10$ GeV	2.8	76	65
$\sum_{jets} \vec{P^T}_{\mathrm{jet}_i} < 100$ GeV	2.5	72	44

	# events			Spread in Stat. 95% C.L.		
	Backgrounds	WZ Signal	$\frac{S}{B}$	λ_Z	$\Delta\kappa_Z$	Δg^1_Z
preselection	1952	3663	1.88	0.014	0.29	0.020
3 leptons, $P^T_{\mathrm{l}^\pm} > 25$ GeV	1359	3285	2.42	0.014	0.29	0.020
$P^T_{\mathrm{miss}} > 25$ GeV	450	2453	5.44	0.014	0.28	0.019
$\lvert M_{\mathrm{l}^+\mathrm{l}^-} - M_{\mathrm{Z}}\rvert < 10$ GeV	144	2331	16.2	0.014	0.29	0.020
$\sum_{jets} \vec{P^T}_{\mathrm{jet}_i} < 100$ GeV	119	1987	16.7	0.013	0.23	0.016

TABLE II: The number of events surviving after each of the kinematic cuts is applied for the WZ analysis. An integrated luminosity $\mathcal{L} = 30$ fb^{-1} at the LHC has been assumed, and reconstruction efficiencies have been applied. The statistical spread in the 95% confidence intervals have been derived using a binned maximum likelihood fit to the $P^T_{\mathrm{Z}^0}$ distribution and the results are averaged over 1000 simulated ATLAS experiments. The numbers reported in this table employ the full NLO simulation for the signal, and a k-factor of 1.5 has been applied to the backgrounds, which are generated at leading order.

C. Event Selection and Efficiency

A preselection is applied immediately after the detector simulation with `ATLfast`. All events satisfying the preselection are written to a computer file for further consideration. The preselection for WZ production requires exactly three isolated high transverse momentum electron or muon type leptons in the region of precision physics ($|\eta| < 2.5$). Two of these leptons must be like flavor and opposite sign. The P^T_{miss} reconstruction must be consistent with the hypothesis that the missing transverse momentum arises from a neutrino which together with one of the charged leptons reconstructs to the W-mass (for a discussion of this reconstruction, refer to the appendix of Ref. [1]), i.e.

$$\begin{array}{l} \underline{WZ \text{ Preselection}} \\ \qquad \text{three isolated electrons or muons, } P^T_{\mathrm{l}^\pm} > 20 \text{ GeV}, \ |\eta_{\mathrm{l}^\pm}| < 2.5 \\ \qquad \text{two of which are like flavor, opposite sign} \\ \qquad \text{solution to neutrino longitudinal momentum exists.} \end{array} \tag{10}$$

The preselection alone is enough to provide an event sample consisting of 65% signal, as shown in the first row of Table II, where the event rates are enumerated for $\mathcal{L} = 30$ fb^{-1}.

Increasing the $P^T_{\mathrm{l}^\pm}$ cut to 25 GeV improves the signal to background ratio (S/B) from 1.9 to 2.4. The P^T_{miss} cut, set at 25 GeV, is effective at greatly reducing the $Z(l^+l^-)$+jet and $ZZ \to l^+l^-l^+l^-$ backgrounds, which do not produce direct neutrinos.

After the transverse momentum cuts, $t\bar{t}$ is the largest background. The charged leptons from this process are usually from W-boson's and not from a Z-boson, so a cut on the mass of the like flavor opposite sign lepton pair is effective at reducing the $t\bar{t}$ background. A window of ± 10 GeV around the Z mass is chosen. The window has been optimised by generating the

$\sum_{jets} \vec{P}^T_{\mathrm{jet}_i}$			Spread in 95% C.L.		
[GeV]	S/B	$S/\sqrt{B}$	λ_Z	$\Delta\kappa_Z$	Δg^1_Z
no cut	16	200	0.0144	0.289	0.0195
< 400	16	190	0.0130	0.263	0.0176
< 300	16	190	0.0131	0.256	0.0172
< 200	16	180	0.0128	0.243	0.0165
< 150	17	190	0.0129	0.239	0.0163
< 100	17	180	0.0130	0.239	0.0161
< 75	18	180	0.0132	0.238	0.0163
< 50	24	200	0.0139	0.246	0.0168
< 40	28	210	0.0141	0.247	0.0171
< 30	30	210	0.0148	0.259	0.0182
< 20	35	210	0.0153	0.273	0.0192
< 10	48	210	0.0168	0.304	0.0218

TABLE III: The effect of the $\sum_{jets} \vec{P}^T_{\mathrm{jet}_i}$ cut on the sensitivity to anomalous TGC's, purity, and significance is tabulated for WZ production. An integrated luminosity of 30 fb^{-1} is assumed and efficiencies have been applied. The statistical spread in the 95% confidence intervals have been derived using a binned maximum likelihood fit to the P^T_{Z} distribution and the results are averaged over 1000 simulated ATLAS experiments.

WZ Selection
three isolated electron or muons, $P^T_{\mathrm{l}^\pm} > 25$ GeV, $\lvert\eta_{\mathrm{l}^\pm}\rvert < 2.5$
two of which are like flavor, opposite sign leptons satisfying
$\lvert M(l^+, l^-) - M_{\mathrm{Z}}\rvert < 10$ GeV
no other charged lepton with $P^T_{\mathrm{l}^\pm} > 20$ GeV, $\lvert\eta_{\mathrm{l}^\pm}\rvert < 2.5$
$P^T_{\mathrm{miss}} > 25$ GeV
$\sum_{jets} \vec{P}^T_{\mathrm{jet}_i} < 100$ GeV
solution to neutrino longitudinal momentum exists

TABLE IV: The kinematic cuts imposed for the WZ analysis are presented.

signal with `PYTHIA` (with includes finite width effects). The NLO simulation of WZ production assumes the narrow width approximation (i.e. the gauge-bosons are always on shell), and so it cannot be used to evaluate width effects. This window, being 20 GeV wide, is sufficiently large that finite width effects are not be important to the signal simulation.

The last cut is a jet veto that operates on the vector sum of the jet activity ($\sum_{jets} \vec{P}^T_{\mathrm{jet}_i}$) in the event, and is chosen so as to optimise the sensitivity to anomalous TGC's in a manner identical to that used for the $W\gamma$ analysis of Ref. [1]. The purpose of the cut is to reduce the effects of NLO corrections, which are largest when there is significant jet activity in the event. The sensitivity to the anomalous TGC's as a function of the vector sum of the jet transverse momentum $\sum_{jets} \vec{P}^T_{\mathrm{jet}_i}$ is shown in Table III. A cut at $\sum_{jets} \vec{P}^T_{\mathrm{jet}_i}$=100 GeV is effective at isolating the region of phase space which is most sensitive to the anomalous TGC's. This is the same cut which has been used in Ref. [1] for $W\gamma$ production—and like that process, this choice does not give the best signal purity, because it is the signal itself which is washing out the sensitivity to the anomalous TGC's.

The final selection cuts are shown in Table IV.

V. ANALYSIS METHODS AND RESULTS

In this section we evaluate the ATLAS experiment's sensitivity to the WWZ anomalous TGC parameters, Δg^1_Z, λ_Z, and $\Delta\kappa_Z$. We start by describing the one and two dimension maximum

likelihood fits which have been used to assess the sensitivity and systematics. Following that, we apply a variation of the Optimal Observables method for hadron colliders, and evaluate its sensitivity. We then compare the various methods, and present the results as a function of integrated luminosity and form factor assumptions. Lastly, we evaluate the potential for directly measuring the energy dependence of the anomalous TGC parameters in the scenario where significant anomalous effects are observed.

A. Measuring Anomalous Coupling Parameters and Evaluating Systematics

The expected statistical confidence intervals for the anomalous TGC parameters are evaluated by comparing histograms of 'mock' ATLAS data (simulated with SM TGC parameters) to reference histograms which are evaluated as a function of the anomalous TGC parameters using a binned maximum likelihood fit to one or two dimension distributions. The distributions which have been studied are enumerated in Table V. Many of the methods which will be discussed in this section will require the reconstruction of event kinematics, including the four momentum of the final state neutrino from the W-decay. Normally there are two solutions for the neutrino four momentum. This reconstruction is complicated and is discussed in the appendix of Ref. [1].

For simplicity, we have reduced the number of anomalous TGC parameters in each fit to either one or two, and set the remaining parameters to their Standard Model values.

As an example of a maximum likelihood fit to a one dimension distribution, the transverse momentum distribution of the Z-boson is shown in Figure 2, after applying the kinematic cuts described in Section IV. The points with error bars represent "mock" data for one ATLAS experiment with integrated luminosity of 30 fb^{-1}. This data has been simulated using the SM TGC parameters, and includes the background contributions. The "mock" data histogram is constructed by sampling each bin according to a Poisson distribution with the mean given by the relevant bin content of the SM reference histogram. The lines in Figure 2 (bottom) are the reference distributions (i.e. theoretical expectation) for several choices of the anomalous TGC parameters. The contribution of backgrounds to the reference distributions is shown as a shaded histogram, and does not depend on the anomalous TGC parameters. The one and two parameter negative log likelihood curves are shown as a function of the λ_Z, Δg_Z^1, and $\Delta\kappa_Z$ parameters with the 68, 90, and 95% confidence limits indicated. These confidence limits correspond to the single experiment which has been simulated for this figure. When another ATLAS experiment is simulated, the confidence limits will be different, on account of statistical fluctuations (indeed it is the sensitivity of the distribution to these fluctuations which the likelihood method measures). In order to obtain the best estimate of the limits that will be achieved at ATLAS, it is necessary to average the confidence limits over many simulated ATLAS experiments (the limits tabulated in this paper are averaged over 5000 simulated experiments).

As an example of a maximum likelihood fit to a two dimension distribution, the transverse momentum of the Z-boson ($P_{\rm Z}^T$) versus the transverse momentum ($P_{\rm l_W^\pm}^T$) of the charged lepton from the W decay is shown in Figure 3, after applying the kinematic cuts described in Section IV. The $P_{\rm Z}^T$ distribution serves to project out the high energy central production region where the anomalous TGC's are enhanced, while the $P_{\rm l_W^\pm}^T$ distribution serves as a projection operator on the gauge-boson helicity states. If the binning of the two dimension distribution of Figure 3 were identical to that of the one dimension of Figure 2, then we would expect better sensitivity from the two dimension one. However, in order to produce the reference histograms for the two dimension histograms in a reasonable amount of computer time, the bin width of the two

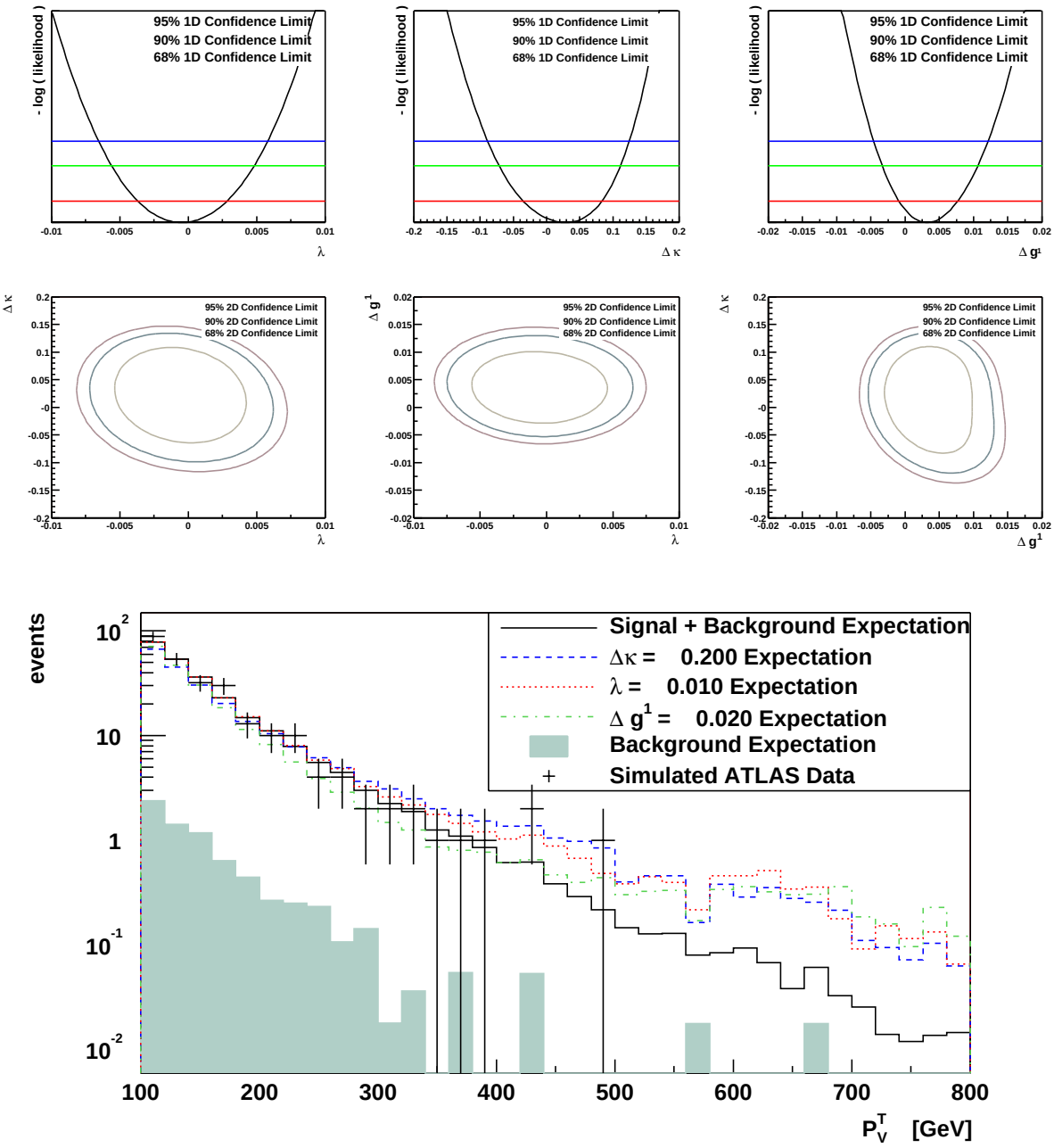

FIG. 2: The transverse momentum distribution of the Z in WZ production is shown (bottom), after applying the kinematic cuts described in Section IV. The points with error bars represent "mock" data for one ATLAS experiment with integrated luminosity of 30 fb^{-1}. This data has been simulated using the SM TGC parameters, and includes the background contributions. The lines are the reference distributions for several choices of the anomalous TGC parameters. The contribution of backgrounds to the reference distributions is shown as a shaded histogram, and does not depend on the anomalous TGC parameters. The one (top three plots) and two (middle three plots) parameter negative log likelihood curves are shown as a function of the λ_Z, $\Delta\kappa_Z$, and Δg_Z^1 parameters with the 68, 90, and 95% confidence limits indicated. These confidence limits correspond to the single experiment which has been simulated for this figure.

	1 dimension distributions	# Bins
P_Z^T	transverse momentum of the Z^0	70
$P_{\mathrm{l}_W}^T$	transverse momentum of the charged lepton from the $W^\pm$ decay	50
P_{miss}^T	missing transverse momentum	50
$\mathrm{mass(WZ)}_{Both\ Sol.}$	diboson invariant mass, each solution is histogrammed with weight $\frac{1}{2}$	100
$\mathrm{mass(WZ)}_{Min}$	smaller of the two solutions for the diboson invariant mass	100
$\mathrm{mass(WZ)}_{Tran}$	$(l_W Z; P_{\mathrm{miss}}^T)$ cluster transverse mass	100
$\eta_{\mathrm{Z}} - \eta_{\mathrm{l}}$	pseudorapidity separation of the γ / Z^0 and the lepton from the $W^\pm$ decay	50
$\cos\theta^*(Z)_{Ave}$	cosine of the production angle for the γ / Z^0 with respect to the beam-line in the reconstructed diboson center-of-mass frame, each of the two solutions are included with weight $\frac{1}{2}$	40
	Optimal Observables	
$\mathrm{Opt\ Obs}(\kappa)_{min\ mass}$	the OO from Eq. 11 using the $\Delta\kappa_Z$ parameter and the ν solution which gives the smaller diboson mass	100
$\mathrm{Opt\ Obs}(\lambda)_{min\ mass}$	the OO from Eq. 11 using the λ_Z parameter and the ν solution which gives the smaller diboson mass	100
$\mathrm{Opt\ Obs}(g^1)_{min\ mass}$	the OO from Eq. 11 using the Δg_Z^1 parameter and the ν solution which gives the smaller diboson mass	100
	2 dimension distributions	
P_Z^T vs. $P_{\mathrm{l}_W}^T$	transverse momentum of the γ / Z^0 vs. transverse momentum of the l_W	14×10
$\mathrm{mass(WZ)}_{Tran}$ vs. $\lvert\eta_{\mathrm{Z}} - \eta_{\mathrm{l}}\rvert$	diboson transverse mass vs. the pseudorapidity separation of the γ / Z^0 and l_W	15×10
$\mathrm{mass(WZ)}_{Both\ Sol.}$ vs. $\cos\theta^*(Z)_{Ave}$	the diboson invariant mass vs. the production angle of the γ / Z^0 in the center-or-mass frame, each of the two solutions are included with weight $\frac{1}{2}$	15×10

TABLE V: Definition of the distributions which are used to extract the confidence intervals for anomalous TGC's in Tables VI-IX. The number of bins used for the histograms of each distribution are shown on the right side of the table.

dimension distributions has been substantially increased.

The systematic uncertainties associated with the measurement of the anomalous TGC parameters using the various one and two dimension distributions have been tabulated in Tables VI and VII.

We estimate the systematic uncertainties by replacing the histograms which represent the

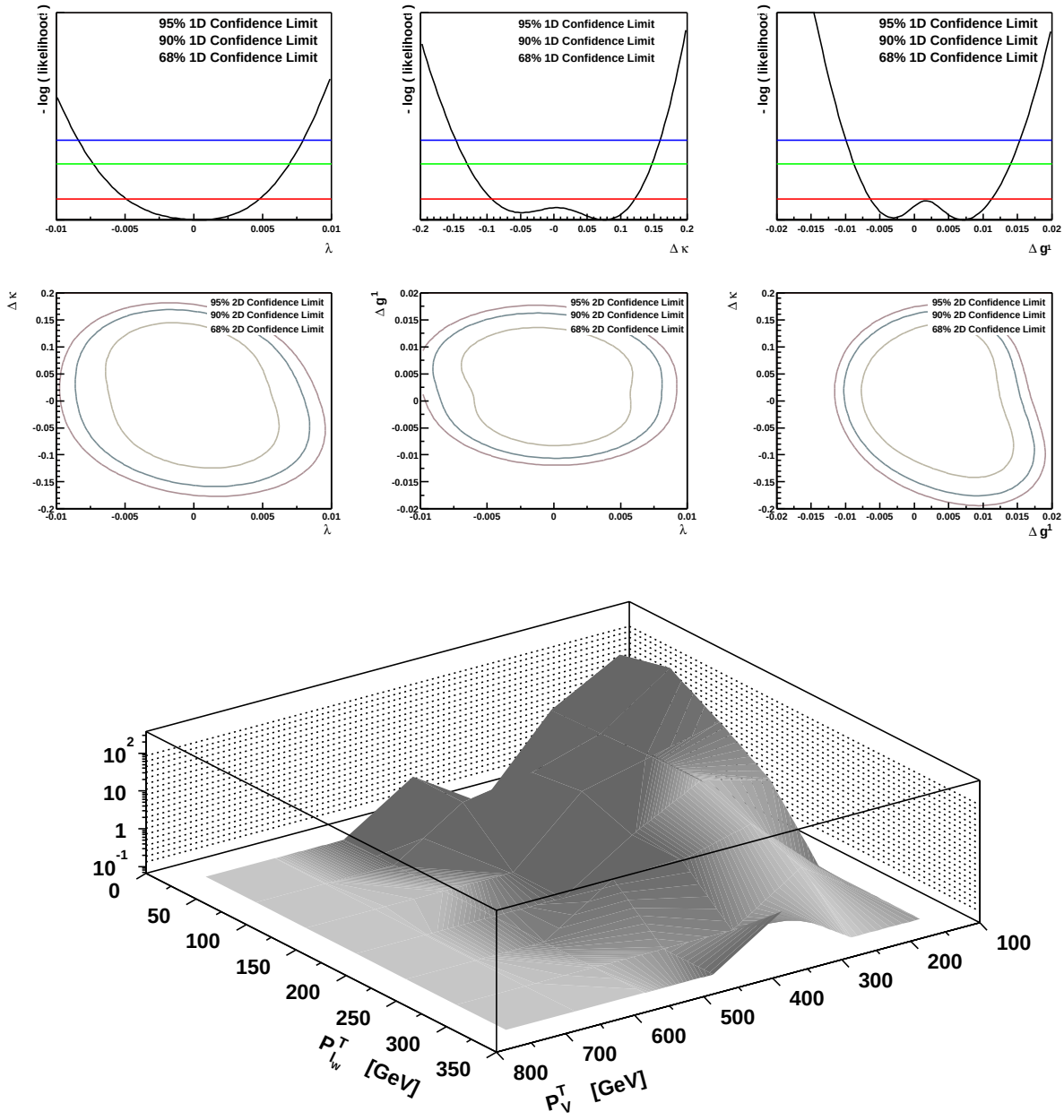

FIG. 3: The transverse momentum of the Z versus the transverse momentum of the charged lepton arising in the $W^{\pm}$ decay distribution for WZ production is shown (bottom), after applying the kinematic cuts described in Section IV. Only the Standard Model reference histogram (including contributions from backgrounds) is shown. The one (top three plots) and two (middle three plots) parameter negative log likelihood curves are shown as a function of the λ_Z, $\Delta\kappa_Z$, and Δg_Z^1 parameters with the 68, 90, and 95% confidence limits indicated. These confidence limits correspond to the single experiment which has been simulated for this figure.

		Background	PDF	Scale	Detector	$\oplus$All
		$k=2,\ k=1$		$\times 2,\ \times \frac{1}{2}$		Systematics
P_Z^T	λ	2e-05,-4e-05	0.00259	0.00156,-0.00175	0.00052	(-0.00317,0.00307)
		(-4e-05,2e-05)	(-0.00259,0.00259)	(-0.00175,0.00156)	(-0.00052,0.00052)	$\Delta\sigma_{\rm syst} = \pm 0.000612$
P_Z^T	$\Delta\kappa$	0.00706,-0.00749	-0.0778	-0.009,-0.009	0.0357	(-0.0864,0.0864)
		(-0.00749,0.00706)	(-0.0778,0.0778)	(-0.009,0.009)	(-0.0357,0.0357)	$\Delta\sigma_{\rm syst} = \pm 0.0215$
P_Z^T	Δg^1	0.00019,-0.00019	-0.00332	-0.0014,-0.00071	0.00594	(-0.00695,0.00695)
		(-0.00019,0.00019)	(-0.00332,0.00332)	(-0.0014,0.0014)	(-0.00594,0.00594)	$\Delta\sigma_{\rm syst} = \pm 0.000734$
$P_{l_W}^T$	λ	0.00032,-0.00042	0.00634	-0.00083,-0.00052	0.00038	(-0.00642,0.00641)
		(-0.00042,0.00032)	(-0.00634,0.00634)	(-0.00083,0.00083)	(-0.00038,0.00038)	$\Delta\sigma_{\rm syst} = \pm 0.000849$
$P_{l_W}^T$	$\Delta\kappa$	0.012,-0.0103	-0.0732	0.00763,-0.0225	0.0459	(-0.0898,0.0875)
		(-0.0103,0.012)	(-0.0732,0.0732)	(-0.0225,0.00763)	(-0.0459,0.0459)	$\Delta\sigma_{\rm syst} = \pm 0.00508$
$P_{l_W}^T$	Δg^1	0.00044,-0.00041	-0.00552	0.00104,-0.00095	0.00764	(-0.00948,0.00949)
		(-0.00041,0.00044)	(-0.00552,0.00552)	(-0.00095,0.00104)	(-0.00764,0.00764)	$\Delta\sigma_{\rm syst} = \pm 0.000283$
$P_{\rm miss}^T$	λ	-0.00037,0.00066	0.00427	0.00087,0.00127	0.00031	(-0.00448,0.00451)
		(-0.00037,0.00066)	(-0.00427,0.00427)	(-0.00127,0.00127)	(-0.00031,0.00031)	$\Delta\sigma_{\rm syst} = \pm 0.00111$
$P_{\rm miss}^T$	$\Delta\kappa$	-0.00499,0.00645	-0.0869	-0.00758,-0.00758	0.0514	(-0.101,0.101)
		(-0.00499,0.00645)	(-0.0869,0.0869)	(-0.00758,0.00758)	(-0.0514,0.0514)	$\Delta\sigma_{\rm syst} = \pm 0.0279$
$P_{\rm miss}^T$	Δg^1	3e-05,-3e-05	-0.00582	-0.00055,0.001	0.0082	(-0.0101,0.0101)
		(-3e-05,3e-05)	(-0.00582,0.00582)	(-0.00055,0.001)	(-0.0082,0.0082)	$\Delta\sigma_{\rm syst} = \pm 0.00068$
mass(WZ)$_{Both\ Sol.}$	λ	2e-05,-0.00069	0.00832	-0.00208,-0.00146	0.00552	(-0.0102,0.0102)
		(-0.00069,2e-05)	(-0.00832,0.00832)	(-0.00208,0.00208)	(-0.00552,0.00552)	$\Delta\sigma_{\rm syst} = \pm 0.000423$
mass(WZ)$_{Both\ Sol.}$	$\Delta\kappa$	0.00548,-0.00591	-0.129	-0.0258,-0.0191	0.129	(-0.185,0.185)
		(-0.00591,0.00548)	(-0.129,0.129)	(-0.0258,0.0258)	(-0.129,0.129)	$\Delta\sigma_{\rm syst} = \pm 0.0316$
mass(WZ)$_{Both\ Sol.}$	Δg^1	0.00056,-0.00052	-0.0102	-0.00431,-0.00228	0.0122	(-0.0165,0.0165)
		(-0.00052,0.00056)	(-0.0102,0.0102)	(-0.00431,0.00431)	(-0.0122,0.0122)	$\Delta\sigma_{\rm syst} = \pm 0.00293$
mass(WZ)$_{Min}$	λ	6e-05,-0.00056	0.00768	-0.00108,0.00083	0.00318	(-0.0084,0.00835)
		(-0.00056,6e-05)	(-0.00768,0.00768)	(-0.00108,0.00083)	(-0.00318,0.00318)	$\Delta\sigma_{\rm syst} = \pm 0.000428$
mass(WZ)$_{Min}$	$\Delta\kappa$	0.00772,-0.00801	-0.109	0.00303,-0.0081	-0.0504	(-0.12,0.12)
		(-0.00801,0.00772)	(-0.109,0.109)	(-0.0081,0.00303)	(-0.0504,0.0504)	$\Delta\sigma_{\rm syst} = \pm 0.0304$
mass(WZ)$_{Min}$	Δg^1	0.00061,-0.00055	-0.00868	-0.00173,-0.0011	-0.00388	(-0.00968,0.00968)
		(-0.00055,0.00061)	(-0.00868,0.00868)	(-0.00173,0.00173)	(-0.00388,0.00388)	$\Delta\sigma_{\rm syst} = \pm 0.00103$
mass(WZ)$_{Tran}$	λ	0.00026,-0.00066	0.00757	0.00236,0.00229	-0.00161	(-0.00812,0.0081)
		(-0.00066,0.00026)	(-0.00757,0.00757)	(-0.00236,0.00236)	(-0.00161,0.00161)	$\Delta\sigma_{\rm syst} = \pm 0.00105$
mass(WZ)$_{Tran}$	$\Delta\kappa$	0.015,-0.0128	-0.11	0.00884,0.0147	-0.00878	(-0.112,0.112)
		(-0.0128,0.015)	(-0.11,0.11)	(-0.0147,0.0147)	(-0.00878,0.00878)	$\Delta\sigma_{\rm syst} = \pm 0.0294$
mass(WZ)$_{Tran}$	Δg^1	0.00064,-0.00056	-0.00865	0.00105,0.0011	-0.00036	(-0.00875,0.00875)
		(-0.00056,0.00064)	(-0.00865,0.00865)	(-0.0011,0.0011)	(-0.00036,0.00036)	$\Delta\sigma_{\rm syst} = \pm 0.000461$

TABLE VI: The systematic errors for the WZ production anomalous TGC parameters at the LHC are enumerated (continued in Table VII). The precision to which the systematic errors are known is denoted by $\Delta\sigma_{\rm syst}$ in the last column. Some of the systematic effects produce a shift which goes only in one direction (i.e. a variation of the scale up or down by a factor 2, shifts the $\Delta\kappa_Z$ parameter in the negative direction for both cases). This is because the likelihood function is often-times nearly symmetric about $\Delta\kappa_Z$=0. In cases such as these (or when only a single shift is reported such as for the p.d.f. systematic), the systematic effect is assumed to go in both directions (the systematic errors which have been used in the combination with statistical limits are reported in parentheses).

		Background $k=2,\ k=1$	PDF	Scale $\times 2,\ \times \frac{1}{2}$	Detector	$\oplus$All Systematics
$\eta_Z - \eta_l$	λ	-0.00723,0.00332	-0.0194	0.00561,0.00756	0.00302	(-0.0222,0.0213)
		(-0.00723,0.00332)	(-0.0194,0.0194)	(-0.00756,0.00756)	(-0.00302,0.00302)	$\Delta\sigma_{\rm syst} = \pm 0.00776$
$\eta_Z - \eta_l$	$\Delta\kappa$	-0.0197,0.0222	-0.0935	0.0502,0.00819	0.262	(-0.283,0.283)
		(-0.0197,0.0222)	(-0.0935,0.0935)	(-0.0502,0.0502)	(-0.262,0.262)	$\Delta\sigma_{\rm syst} = \pm 0.011$
$\eta_Z - \eta_l$	Δg^1	-0.00292,0.00328	-0.0136	0.00567,0.0017	0.0296	(-0.0332,0.0333)
		(-0.00292,0.00328)	(-0.0136,0.0136)	(-0.00567,0.00567)	(-0.0296,0.0296)	$\Delta\sigma_{\rm syst} = \pm 0.0019$
$\cos\theta^*(Z)_{Ave}$	λ	-0.00408,0.00295	-0.0103	0.00284,-0.00294	0.00248	(-0.0117,0.0114)
		(-0.00408,0.00295)	(-0.0103,0.0103)	(-0.00294,0.00284)	(-0.00248,0.00248)	$\Delta\sigma_{\rm syst} = \pm 0.0052$
$\cos\theta^*(Z)_{Ave}$	$\Delta\kappa$	-0.0106,0.0114	-0.0402	0.00521,-0.0122	0.232	(-0.236,0.235)
		(-0.0106,0.0114)	(-0.0402,0.0402)	(-0.0122,0.00521)	(-0.232,0.232)	$\Delta\sigma_{\rm syst} = \pm 0.00614$
$\cos\theta^*(Z)_{Ave}$	Δg^1	-0.0014,0.00154	-0.0054	0.00108,-0.00135	0.0269	(-0.0275,0.0275)
		(-0.0014,0.00154)	(-0.0054,0.0054)	(-0.00135,0.00108)	(-0.0269,0.0269)	$\Delta\sigma_{\rm syst} = \pm 0.0008$
Opt Obs$(\lambda)_{min\ mass}$	λ	-0.00151,0.00117	-0.0119	0.00128,2e-05	0.00364	(-0.0126,0.0126)
		(-0.00151,0.00117)	(-0.0119,0.0119)	(-0.00128,0.00128)	(-0.00364,0.00364)	$\Delta\sigma_{\rm syst} = \pm 0.00167$
Opt Obs$(\kappa)_{min\ mass}$	$\Delta\kappa$	-0.0102,0.0116	-0.0829	0.00523,0.00153	0.19	(-0.208,0.208)
		(-0.0102,0.0116)	(-0.0829,0.0829)	(-0.00523,0.00523)	(-0.19,0.19)	$\Delta\sigma_{\rm syst} = \pm 0.00884$
Opt Obs$(g^1)_{min.\ mass}$	Δg^1	-0.0005,0.00053	-0.00844	0.0009,-0.00164	0.0473	(-0.0481,0.048)
		(-0.0005,0.00053)	(-0.00844,0.00844)	(-0.00164,0.0009)	(-0.0473,0.0473)	$\Delta\sigma_{\rm syst} = \pm 0.00141$
P_Z^T vs. $P_{l_W}^T$	λ	-6e-05,-6e-05	0.00284	8e-05,-0.00187	-6e-05	(-0.0034,0.00284)
		(-6e-05,6e-05)	(-0.00284,0.00284)	(-0.00187,8e-05)	(-6e-05,6e-05)	$\Delta\sigma_{\rm syst} = \pm 0.000721$
P_Z^T vs. $P_{l_W}^T$	$\Delta\kappa$	0.0102,-0.00998	-0.00189	0.00358,-0.00075	0.0215	(-0.0238,0.0241)
		(-0.00998,0.0102)	(-0.00189,0.00189)	(-0.00075,0.00358)	(-0.0215,0.0215)	$\Delta\sigma_{\rm syst} = \pm 0.0149$
P_Z^T vs. $P_{l_W}^T$	Δg^1	0.00024,-0.00025	-0.00197	0.00087,0.00183	0.00508	(-0.00575,0.00575)
		(-0.00025,0.00024)	(-0.00197,0.00197)	(-0.00183,0.00183)	(-0.00508,0.00508)	$\Delta\sigma_{\rm syst} = \pm 0.000971$
mass(WZ)$_{Tran}$	λ	-0.00021,0.00026	0.00313	-0.00096,0.00191	0.00123	(-0.0035,0.00388)
vs. $\lvert\eta_Z - \eta_l\rvert$		(-0.00021,0.00026)	(-0.00313,0.00313)	(-0.00096,0.00191)	(-0.00123,0.00123)	$\Delta\sigma_{\rm syst} = \pm 0.000738$
mass(WZ)$_{Tran}$	$\Delta\kappa$	-0.00199,0.00233	-0.0658	0.0138,0.0281	0.101	(-0.124,0.124)
vs. $\lvert\eta_Z - \eta_l\rvert$		(-0.00199,0.00233)	(-0.0658,0.0658)	(-0.0281,0.0281)	(-0.101,0.101)	$\Delta\sigma_{\rm syst} = \pm 0.00503$
mass(WZ)$_{Tran}$	Δg^1	4e-05,-5e-05	-0.00249	0.00028,-0.00017	0.0106	(-0.0109,0.0109)
vs. $\lvert\eta_Z - \eta_l\rvert$		(-5e-05,4e-05)	(-0.00249,0.00249)	(-0.00017,0.00028)	(-0.0106,0.0106)	$\Delta\sigma_{\rm syst} = \pm 0.000344$
mass(WZ)$_{Min}$	λ	-0.00024,0.0003	0.00328	0.00042,0.00042	0.00134	(-0.00358,0.00358)
vs. $\lvert\eta_Z - \eta_l\rvert$		(-0.00024,0.0003)	(-0.00328,0.00328)	(-0.00042,0.00042)	(-0.00134,0.00134)	$\Delta\sigma_{\rm syst} = \pm 0.000895$
mass(WZ)$_{Min}$	$\Delta\kappa$	-0.00274,0.00326	-0.0621	0.00722,0.00626	0.102	(-0.12,0.12)
vs. $\lvert\eta_Z - \eta_l\rvert$		(-0.00274,0.00326)	(-0.0621,0.0621)	(-0.00722,0.00722)	(-0.102,0.102)	$\Delta\sigma_{\rm syst} = \pm 0.0117$
mass(WZ)$_{Min}$	Δg^1	2e-05,-2e-05	-0.00263	0.00033,0.00092	0.0108	(-0.0112,0.0112)
vs. $\lvert\eta_Z - \eta_l\rvert$		(-2e-05,2e-05)	(-0.00263,0.00263)	(-0.00092,0.00092)	(-0.0108,0.0108)	$\Delta\sigma_{\rm syst} = \pm 0.000374$
mass(WZ)$_{Both\ Sol.}$	λ	-0.00027,0.00032	-0.00349	0.00125,0.00129	0.00125	(-0.00393,0.00394)
vs. $\cos\theta^*(Z)_{Ave}$		(-0.00027,0.00032)	(-0.00349,0.00349)	(-0.00129,0.00129)	(-0.00125,0.00125)	$\Delta\sigma_{\rm syst} = \pm 0.00082$
mass(WZ)$_{Both\ Sol.}$	$\Delta\kappa$	-0.00347,0.00397	-0.0584	-0.00305,-0.00946	0.105	(-0.12,0.12)
vs. $\cos\theta^*(Z)_{Ave}$		(-0.00347,0.00397)	(-0.0584,0.0584)	(-0.00946,0.00946)	(-0.105,0.105)	$\Delta\sigma_{\rm syst} = \pm 0.00535$
mass(WZ)$_{Both\ Sol.}$	Δg^1	-4e-05,4e-05	-0.0032	9e-05,9e-05	0.0118	(-0.0122,0.0122)
vs. $\cos\theta^*(Z)_{Ave}$		(-4e-05,4e-05)	(-0.0032,0.0032)	(-9e-05,9e-05)	(-0.0118,0.0118)	$\Delta\sigma_{\rm syst} = \pm 0.000319$

TABLE VII: Continuation of Table VI.

'mock' ATLAS data with histograms which use a different model assumption. The reference histogram assumptions are not changed. The change in the model assumptions causes a shift in the preferred value for each anomalous TGC parameter. This shift is independent of luminosity. This is taken as a pessimistic estimate of the systematic error, since it is likely that it will be possible to extract corrections for many of these systematic effects directly from the LHC data.

We have studied the following systematic effects: (1) Background rate systematics are evaluated by varying the background process k-factor in the 'mock' data histograms from 1.5 up to 2 and down to 1. (2) Parton density function systematics are evaluated by replacing the CTEQ4 p.d.f.'s which have been used for the all simulations with the CTEQ3 [23] series p.d.f.'s in the 'mock' data histograms. (3) Systematics arising from neglected higher orders are evaluated by varying the renormalisation and factorisation scales up and down by a factor 2 for the WZ signal simulation. (4) Detector related systematics are evaluated by simply turning off the detector smearing in the event generation software chain, which represents the shift in the results that would arise if the ATLAS detector were to be replaced by a fictional 'perfect' detector.

The systematic effects are uncorrelated, and so the individual shifts are added together in quadrature to obtain the total systematic error for the measurements. Further details about the maximum likelihood fit, treatment of systematics, and the construction of reference histograms as a function of the anomalous TGC parameters are discussed in Ref. [1].

B. Optimal Observables

Certain kinematic observables are more sensitive to anomalous TGC's than others, because these distributions are able to project out more information which is relevant for the couplings. The method of Optimal Observables (OO) [24] attempts to project onto a single variable the kinematic information which is most sensitive to a particular anomalous TGC parameter. This method has been used extensively by the LEP collaborations for TGC measurements [25–28].

Optimal Observables have not previously been applied to TGC studies in hadronic collisions that we are aware of. In this section, the OO equations for e^+e^- collisions are generalised to hadron collisions in the simplest possible way, and the sensitivity of the OO method to the anomalous TGC parameters is investigated.

Each anomalous TGC has its own OO. The OO for the λ_Z parameter of a given event is

$$\mathrm{OO}_{\lambda_Z} \;=\; \lim_{\lambda_Z \to 0} \frac{d\sigma(\mathrm{SM}+\lambda_Z) - d\sigma(\mathrm{SM})}{\lambda_Z \; d\sigma(\mathrm{SM})} \tag{11}$$

where $d\sigma$ is the differential cross section (i.e. probability) for the event to have occurred. The OO for λ_Z is the relative change in the event probability when the λ_Z parameter is moved from its SM value by some small amount λ_Z. Note that OO_{λ_Z} does not depend on λ_Z.

The differential cross section depends on the identity and kinematic configuration of all the particles involved in the reaction. For a process like $e^+e^- \to W^+W^- \to q\bar{q}'l^-\bar{\nu}$, $d\sigma$ can be directly evaluated by restricting the calculation to the leading order, and using the Born level matrix elements ($d\sigma$ appears as a ratio, so overall factors can be neglected).

For the case of hadronic $W^\pm Z$ production, $d\sigma$ depends on the kinematic configuration and flavor of the $q, \bar{q}', l^\pm, \nu, l^+, l^-$ particles. This complicates the application of Optimal Observables, because there are two solutions for the neutrino momentum, the flavor of the quarks which participate in the hard subprocess is unknown, and there is a further twofold ambiguity as to whether the q ($\bar{q}'$) has origin in the forward or backward proton beam. Yet another complication

is that QCD corrections are large at hadron colliders, and the OO method derived here makes use of leading order matrix elements only.

These complications will wash out the sensitivity of the Optimal Observables method for hadronic collisions. The goal of this study is to investigate the feasibility of the OO method in the face of these challenges.

To evaluate the OO of Eq. 11, the neutrino solution which gives the minimum diboson invariant mass (motivated by the study included in the appendix of Ref. [1]) has been used, and all other ambiguities have been summed over, exactly as is normal for the calculation of event weights in a Monte Carlo event generator. The differential cross section for each $W^{\pm}Z$ event is

$$d\sigma \propto \sum^{\text{quark flavors}} \Big[f_{\mathrm{p}_1\to\mathrm{q}}(x,Q^2) f_{\mathrm{p}_2\to\bar{\mathrm{q}}}(x,Q^2) |\mathcal{M}^2_{\mathrm{q}\bar{\mathrm{q}}'\to \mathrm{l}^{\pm}\nu\mathrm{l}^{+}\mathrm{l}^{-}}| + f_{\mathrm{p}_1\to\bar{\mathrm{q}}}(x,Q^2) f_{\mathrm{p}_2\to\mathrm{q}}(x,Q^2) |\mathcal{M}^2_{\bar{\mathrm{q}}'\mathrm{q}\to \mathrm{l}^{\pm}\mathrm{l}^{+}\mathrm{l}^{-}}| \Big] \quad (12)$$

where $f_{\mathrm{p_i}\to\overset{(-)}{\mathrm{q}}}(x,Q^2)$ is the structure function of the p_i beam, and reflects the probability of resolving parton $\overset{(-)}{q}$ in the beam at Bjorken momentum fraction x and scale Q. The Born level matrix element ($\mathcal{M}$) expressions of Ref. [29] have been used for the evaluation of $d\sigma$.

The effect non-standard couplings have on the OO distributions is shown in Figure 4, using the OO's calculated according to Eq. 12. The anomalous TGC parameters employed for these plots have been chosen such that the effects of the non-standard couplings are clearly visible, and the effect of the individual parameters on the OO distributions should not be compared directly since different values of the parameters have been used in each case. In general, non-standard couplings affect the OO distributions most in the region far from zero, as is expected. The OO(Δg_Z^1) distribution appears least sensitive to anomalous TGC's of any type. An important difference between these OO distributions and the OO distributions obtained at e^+e^- experiments (e.g. LEP) is that the mean of the distributions shown in Figure 4 is not very sensitive to anomalous TGC's (the distributions are plotted on a logarithmic scale). This implies that the technique used at LEP, wherein the mean values of the distributions are tabulated as a function of the anomalous TGC's, will not be feasible at hadron colliders, where the centre-of-mass energy varies event by event.

The OO($\Delta\kappa_Z$) distribution for WZ production at the LHC is shown in Figure 5, including detector effects and the contribution from backgrounds. The expectation for SM couplings and three choices of anomalous TGC's are indicated. 'Mock' data from one simulated ATLAS experiment is superimposed and the corresponding likelihood curves are shown. The events which populate the regions of OO($\Delta\kappa_Z$) far from zero are most sensitive to changes in the $\Delta\kappa_Z$ parameter.

Measurements and confidence limits can be calculated for the anomalous TGC parameters using a binned maximum likelihood fit to the OO distributions in the same manner presented in Sec. V A for other one dimension distributions. The location of the OO distribution mean is not a very sensitive way of measuring the anomalous TGC's at hadron colliders. The confidence intervals for the Optimal Observables method will be compared to other methods in the following section.

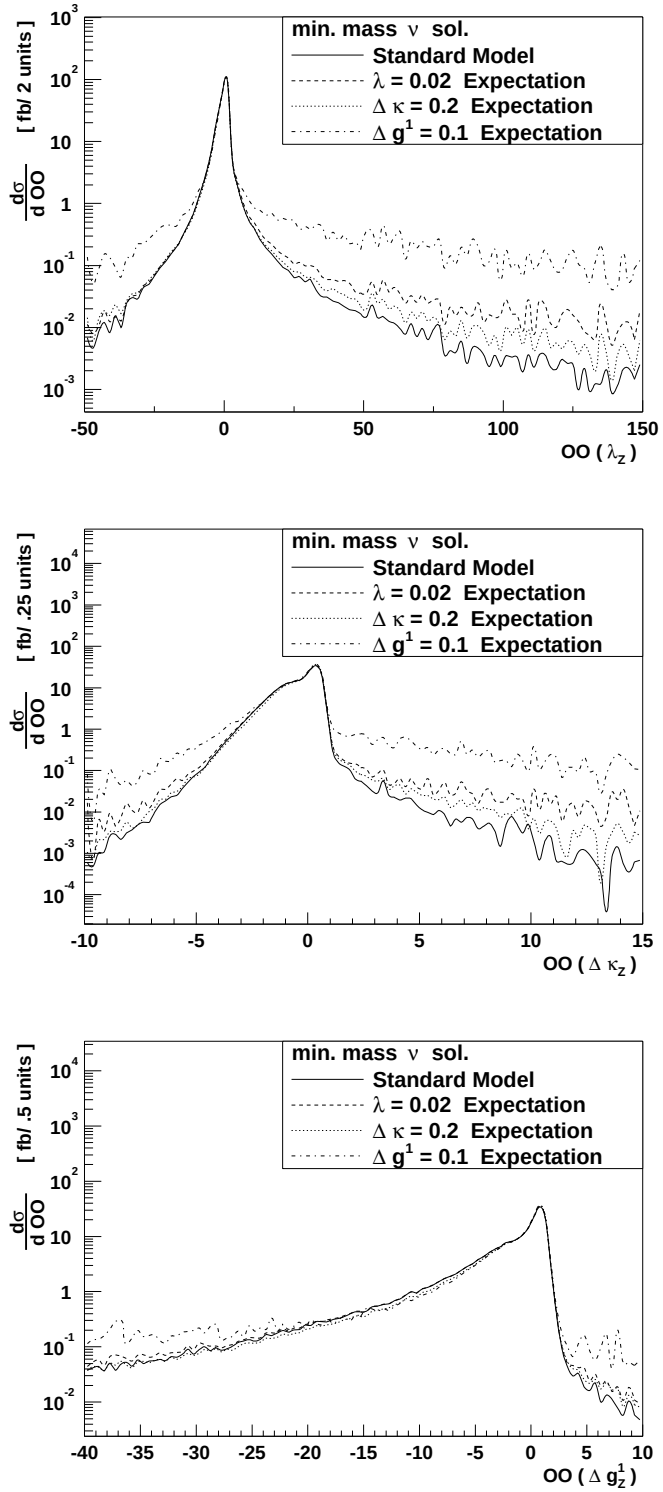

FIG. 4: The dependence of the λ_Z Optimal Observable (top), $\Delta\kappa_Z$ Optimal Observable (middle), and Δg_Z^1 Optimal Observable (bottom) on the anomalous TGC parameters are shown for WZ production at the LHC. The irregularities in the tails of the distributions are caused by low Monte Carlo simulation statistics in this region, and are not physical in nature.

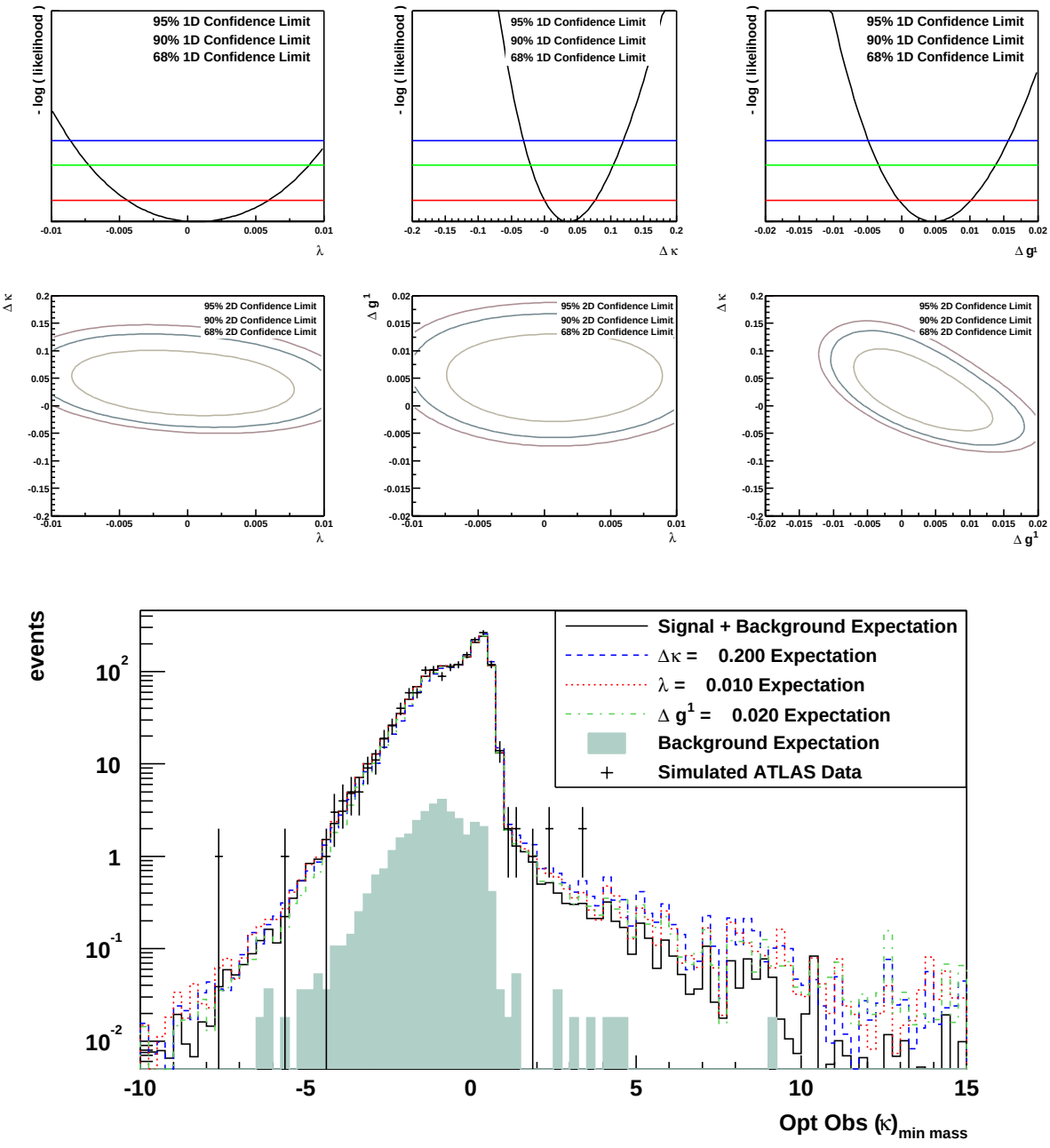

FIG. 5: The distribution of the $\Delta\kappa_Z$ Optimal Observable in WZ production is shown (bottom), after applying the kinematic cuts described in Section IV. The points with error bars represent "mock" data for one ATLAS experiment with integrated luminosity of 30 fb^{-1}. This data has been simulated using the SM TGC parameters, and includes the background contributions. The lines are the reference distributions for several choices of the anomalous TGC parameters. The contribution of backgrounds to the reference distributions is shown as a shaded histogram, and does not depend on the anomalous TGC parameters. The one (top three plots) and two (middle three plots) parameter negative log likelihood curves are shown as a function of the λ_Z, $\Delta\kappa_Z$, and Δg_Z^1 parameters with the 68, 90, and 95% confidence limits indicated. These confidence limits correspond to the single experiment which has been simulated for this figure.

C. Results and Comparison of Methods

Having discussed and evaluated the systematic errors and the techniques used to extract the anomalous TGC parameters, we are in a position to compare the analysis methods. We will quantify the sensitivity of the methods by the spread in the 95% confidence intervals. For example, the $P_{\rm Z}^T$ distribution has a statistical confidence interval of $-0.0065 < \lambda_Z < 0.0066$, which amounts to a spread of 0.0131. After adding the effects of systematics in quadrature, this spread increases to 0.0145. The confidence intervals for all of the distributions (see Table V for a summary of the distribution definitions) studied in this paper are presented in Tables VIII and IX.

The transverse momentum of the Z-boson ($P_{\rm Z}^T$) has been the traditional means of extracting limits on the anomalous TGC's at hadron colliders because it can be reconstructed directly from the charged lepton four-momenta (without the assumptions necessary for reconstructing the neutrino four-momentum) and it projects out the central, high energy production regime where the anomalous TGC's are enhanced.

For the λ_Z parameter, a fit to the one dimension $P_{\rm Z}^T$ distribution gives the best statistical and total confidence intervals. However, the statistical confidence intervals for the two dimension distributions are only slightly worse. The $P_{\rm Z}^T$ versus $P_{\rm l_W}^T$ two dimension distribution is particularly promising, since it shows very little sensitivity to systematic effects. This 2-dimension distribution uses a coarse binning granularity which keeps it from showing an improvement over the single dimension $P_{\rm Z}^T$ distribution.

The limits derived from the OO(λ_Z) Optimal Observable distributions are not competitive with the limits derived from the $P_{\rm Z}^T$ distribution. The OO distributions require significant reconstruction and theoretical input: to calculate the OO for a particular event, the centre-of-mass system needs to be fully reconstructed such that all particle momenta are known, and phenomenological parton density functions are included in the calculation. The measurement of $P_{\rm Z}^T$ is robust and simple, requiring only the reconstruction of the transverse momentum of the charged leptons from the Z decay. Another important attribute of the $P_{\rm Z}^T$ observable is that its functional form ($P_{\rm Z}^T = |p_Z| \sin\theta_Z$) is very similar to the functional form which would be expected for OO(λ_Z). This is apparent from the approximate equations for $\Delta\mathcal{M}$ presented in Equations. 5-8, where the dominant change in the Born level matrix element at high energy arising from the λ_Z parameter is seen to be proportional to $\hat{s}\sin\theta_Z$. This is the reason the $P_{\rm Z}^T$ is so sensitive to the λ_Z parameter—it is an easily reconstructed observable which is functionally similar to our expectation for an λ_Z Optimal Observable.

The expected 95% confidence intervals for the λ_Z parameter using a maximum likelihood fit to the $P_{\rm Z}^T$ distribution is

$$-0.0065_{\rm stat.},\quad -0.0032_{\rm syst.} < \lambda_Z < +0.0066_{\rm stat.},\quad +0.0031_{\rm syst.} \tag{13}$$

which gives

$$-0.0073 < \lambda_Z < 0.0073 \tag{14}$$

when the statistical and systematic contributions are added in quadrature. The dominant systematic effects are theoretical, with the parton density functions providing the biggest contribution.

The $\Delta\kappa_Z$ parameter enters the matrix elements proportional to $\sqrt{\hat{s}}(1 \mp \cos\theta_Z^\star)$, and so it does not exhibit the same enhancements in the central region that the λ_Z parameter does. It is, however, very sensitive to the helicity of the W-boson, because it appears only in the

	95% Statistical Limit	⊕All Systematics	95% Confidence Limit (stat⊕syst)
P_Z^T	-0.00652< λ <0.0066	(-0.00317,0.00307)	-0.00725< λ <0.00727
	λ spread= 0.0131		λ spread= 0.0145
P_Z^T	-0.113< $\Delta\kappa$ <0.126	(-0.0864,0.0864)	-0.143< $\Delta\kappa$ <0.153
	$\Delta\kappa$ spread= 0.239		$\Delta\kappa$ spread= 0.295
P_Z^T	-0.00641< Δg^1 <0.00972	(-0.00695,0.00695)	-0.00945< Δg^1 <0.012
	Δg^1 spread= 0.0161		Δg^1 spread= 0.0214
$P_{\mathrm{l}_W}^T$	-0.00823< λ <0.00844	(-0.00642,0.00641)	-0.0104< λ <0.0106
	λ spread= 0.0167		λ spread= 0.021
$P_{\mathrm{l}_W}^T$	-0.0757< $\Delta\kappa$ <0.129	(-0.0898,0.0875)	-0.117< $\Delta\kappa$ <0.156
	$\Delta\kappa$ spread= 0.205		$\Delta\kappa$ spread= 0.273
$P_{\mathrm{l}_W}^T$	-0.00666< Δg^1 <0.0111	(-0.00948,0.00949)	-0.0116< Δg^1 <0.0146
	Δg^1 spread= 0.0178		Δg^1 spread= 0.0262
P_{miss}^T	-0.0083< λ <0.00836	(-0.00448,0.00451)	-0.00944< λ <0.0095
	λ spread= 0.0167		λ spread= 0.0189
P_{miss}^T	-0.0857< $\Delta\kappa$ <0.139	(-0.101,0.101)	-0.133< $\Delta\kappa$ <0.172
	$\Delta\kappa$ spread= 0.225		$\Delta\kappa$ spread= 0.305
P_{miss}^T	-0.00699< Δg^1 <0.0119	(-0.0101,0.0101)	-0.0123< Δg^1 <0.0156
	Δg^1 spread= 0.0189		Δg^1 spread= 0.0279
mass(WZ)$_{Both\ Sol.}$	-0.00912< λ <0.00947	(-0.0102,0.0102)	-0.0137< λ <0.0139
	λ spread= 0.0186		λ spread= 0.0276
mass(WZ)$_{Both\ Sol.}$	-0.105< $\Delta\kappa$ <0.15	(-0.185,0.185)	-0.213< $\Delta\kappa$ <0.238
	$\Delta\kappa$ spread= 0.255		$\Delta\kappa$ spread= 0.45
mass(WZ)$_{Both\ Sol.}$	-0.00914< Δg^1 <0.0142	(-0.0165,0.0165)	-0.0189< Δg^1 <0.0218
	Δg^1 spread= 0.0234		Δg^1 spread= 0.0407
mass(WZ)$_{Min}$	-0.00826< λ <0.00829	(-0.0084,0.00835)	-0.0118< λ <0.0118
	λ spread= 0.0166		λ spread= 0.0236
mass(WZ)$_{Min}$	-0.089< $\Delta\kappa$ <0.129	(-0.12,0.12)	-0.15< $\Delta\kappa$ <0.176
	$\Delta\kappa$ spread= 0.218		$\Delta\kappa$ spread= 0.326
mass(WZ)$_{Min}$	-0.00753< Δg^1 <0.012	(-0.00968,0.00968)	-0.0123< Δg^1 <0.0154
	Δg^1 spread= 0.0195		Δg^1 spread= 0.0277
mass(WZ)$_{Tran}$	-0.00775< λ <0.00787	(-0.00812,0.0081)	-0.0112< λ <0.0113
	λ spread= 0.0156		λ spread= 0.0225
mass(WZ)$_{Tran}$	-0.0859< $\Delta\kappa$ <0.129	(-0.112,0.112)	-0.141< $\Delta\kappa$ <0.171
	$\Delta\kappa$ spread= 0.215		$\Delta\kappa$ spread= 0.312
mass(WZ)$_{Tran}$	-0.00703< Δg^1 <0.0114	(-0.00875,0.00875)	-0.0112< Δg^1 <0.0144
	Δg^1 spread= 0.0184		Δg^1 spread= 0.0256
$\eta_{\mathrm{Z}} - \eta_{\mathrm{l}}$	-0.0256< λ <0.0305	(-0.0222,0.0213)	-0.0339< λ <0.0372
	λ spread= 0.0562		λ spread= 0.0712
$\eta_{\mathrm{Z}} - \eta_{\mathrm{l}}$	-0.134< $\Delta\kappa$ <0.201	(-0.283,0.283)	-0.313< $\Delta\kappa$ <0.347
	$\Delta\kappa$ spread= 0.335		$\Delta\kappa$ spread= 0.660
$\eta_{\mathrm{Z}} - \eta_{\mathrm{l}}$	-0.0184< Δg^1 <0.0561	(-0.0332,0.0333)	-0.038< Δg^1 <0.0652
	Δg^1 spread= 0.0745		Δg^1 spread= 0.103

TABLE VIII: The 95% confidence intervals for WZ production anomalous TGC parameters at the LHC assuming an integrated luminosity of 30 fb^{-1} (continued in Table IX).

	95% Statistical Limit	⊕All Systematics	95% Confidence Limit (stat⊕syst)
$\cos\theta^*(Z)_{Ave}$	-0.0198< λ <0.0237	(-0.0117,0.0114)	-0.023< λ <0.0262
	λ spread= 0.0434		λ spread= 0.0492
$\cos\theta^*(Z)_{Ave}$	-0.0942< $\Delta\kappa$ <0.142	(-0.236,0.235)	-0.254< $\Delta\kappa$ <0.275
	$\Delta\kappa$ spread= 0.236		$\Delta\kappa$ spread= 0.529
$\cos\theta^*(Z)_{Ave}$	-0.0131< Δg^1 <0.0416	(-0.0275,0.0275)	-0.0304< Δg^1 <0.0499
	Δg^1 spread= 0.0548		Δg^1 spread= 0.0803
Opt Obs$(\lambda)_{min\ mass}$	-0.0123< λ <0.0108	(-0.0126,0.0126)	-0.0176< λ <0.0166
	λ spread= 0.0231		λ spread= 0.0342
Opt Obs$(\kappa)_{min\ mass}$	-0.0662< $\Delta\kappa$ <0.0893	(-0.208,0.208)	-0.218< $\Delta\kappa$ <0.226
	$\Delta\kappa$ spread= 0.156		$\Delta\kappa$ spread= 0.445
Opt Obs$(g^1)_{min.\ mass}$	-0.0106< Δg^1 <0.0139	(-0.0481,0.048)	-0.0492< Δg^1 <0.05
	Δg^1 spread= 0.0245		Δg^1 spread= 0.0992
P_Z^T vs. $P_{l_W}^T$	-0.00666< λ <0.00667	(-0.0034,0.00284)	-0.00748< λ <0.00725
	λ spread= 0.0133		λ spread= 0.0147
P_Z^T vs. $P_{l_W}^T$	-0.104< $\Delta\kappa$ <0.122	(-0.0238,0.0241)	-0.106< $\Delta\kappa$ <0.124
	$\Delta\kappa$ spread= 0.225		$\Delta\kappa$ spread= 0.231
P_Z^T vs. $P_{l_W}^T$	-0.00641< Δg^1 <0.00999	(-0.00575,0.00575)	-0.00861< Δg^1 <0.0115
	Δg^1 spread= 0.0164		Δg^1 spread= 0.0201
mass(WZ)$_{Tran}$	-0.00678< λ <0.00682	(-0.0035,0.00388)	-0.00763< λ <0.00784
vs. $\lvert\eta_Z - \eta_l\rvert$	λ spread= 0.0136		λ spread= 0.0155
mass(WZ)$_{Tran}$	-0.0702< $\Delta\kappa$ <0.109	(-0.124,0.124)	-0.142< $\Delta\kappa$ <0.165
vs. $\lvert\eta_Z - \eta_l\rvert$	$\Delta\kappa$ spread= 0.18		$\Delta\kappa$ spread= 0.307
mass(WZ)$_{Tran}$	-0.00535< Δg^1 <0.00819	(-0.0109,0.0109)	-0.0121< Δg^1 <0.0136
vs. $\lvert\eta_Z - \eta_l\rvert$	Δg^1 spread= 0.0135		Δg^1 spread= 0.0257
mass(WZ)$_{Min}$	-0.00679< λ <0.00681	(-0.00358,0.00358)	-0.00767< λ <0.0077
vs. $\lvert\eta_Z - \eta_l\rvert$	λ spread= 0.0136		λ spread= 0.0154
mass(WZ)$_{Min}$	-0.0708< $\Delta\kappa$ <0.108	(-0.12,0.12)	-0.139< $\Delta\kappa$ <0.161
vs. $\lvert\eta_Z - \eta_l\rvert$	$\Delta\kappa$ spread= 0.178		$\Delta\kappa$ spread= 0.3
mass(WZ)$_{Min}$	-0.00538< Δg^1 <0.00813	(-0.0112,0.0112)	-0.0124< Δg^1 <0.0138
vs. $\lvert\eta_Z - \eta_l\rvert$	Δg^1 spread= 0.0135		Δg^1 spread= 0.0263
mass(WZ)$_{Both\ Sol.}$	-0.00687< λ <0.00695	(-0.00393,0.00394)	-0.00792< λ <0.00798
vs. $\cos\theta^*(Z)_{Ave}$	λ spread= 0.0138		λ spread= 0.0159
mass(WZ)$_{Both\ Sol.}$	-0.0645< $\Delta\kappa$ <0.0991	(-0.12,0.12)	-0.137< $\Delta\kappa$ <0.156
vs. $\cos\theta^*(Z)_{Ave}$	$\Delta\kappa$ spread= 0.164		$\Delta\kappa$ spread= 0.293
mass(WZ)$_{Both\ Sol.}$	-0.00536< Δg^1 <0.00809	(-0.0122,0.0122)	-0.0134< Δg^1 <0.0147
vs. $\cos\theta^*(Z)_{Ave}$	Δg^1 spread= 0.0135		Δg^1 spread= 0.028

TABLE IX: Continuation of Table VIII.

$H_W = 0$ helicity states. This is evident in the confidence limits (especially for WZ production) where the P_{lW}^T distribution (which acts as a helicity projector) is seen to have similar or greater sensitivity than the P_{Z}^T distribution.

Substantial gains in sensitivity can be achieved for the $\Delta\kappa_Z$ parameter by using analysis techniques which encode more information than simple one dimension distributions do. For the $\Delta\kappa_Z$ parameter, Optimal Observables provide the best limits when statistics are considered alone. However, an improvement in the statistical confidence limits is not enough to justify using an alternative method for extracting the confidence limits—systematic effects also need to be taken into account. Since the calculation of the OO's requires more in the way of reconstruction and phenomenological input, it is expected that these distributions will be more sensitive to systematic effects. Indeed, this is the case. Systematics (and in particular detector related effects) have a substantial effect on the Optimal Observables distributions and dominate the confidence intervals, making the limits not competitive with other methods. If the systematics can be controlled to a degree beyond what has been assumed in this work, Optimal Observables may provide a viable means of measuring the $\Delta\kappa_Z$ parameters at the LHC.

The expected 95% confidence intervals for the $\Delta\kappa_Z$ parameter using a maximum likelihood fit to the two dimension P_{Z}^T vs. P_{lW}^T distribution is

$$-0.10_{\mathrm{stat.}},\quad -0.024_{\mathrm{syst.}} < \Delta\kappa_Z < +0.12_{\mathrm{stat.}},\quad +0.024_{\mathrm{syst.}} \tag{15}$$

which gives

$$-0.11 < \Delta\kappa_Z < 0.12 \tag{16}$$

when the statistical and systematic contributions are added in quadrature.

The Δg_Z^1 parameter sensitivity behaves very differently from the other parameters, since this anomalous coupling parameter is more sensitive to systematic effects.

Because of the energy squared enhancement the Δg_Z^1 coupling receives in the $(H_Z, H_W) = (0,0)$ helicity state, the statistical confidence limits for Δg_Z^1 are comparable to the λ_Z statistical limits. The best distribution for measuring the Δg_Z^1 parameter is the P_{Z}^T vs. P_{lW}^T distribution, which gives the most stringent statistical and total confidence intervals. Comparable sensitivity is obtained with the one dimension P_{Z}^T distribution.

In all cases the systematic contribution is comparable with the statistical contribution, and so a careful understanding and evaluation of the systematic uncertainties will be particularly important for measurements of this parameter at the LHC. The dominant systematic effect comes from our theoretical understanding of the proton structure (p.d.f.'s). Detector related systematic effects will be of importance for measurements of this parameter, particularly if two dimension distributions are employed.

The expected 95% confidence intervals for the Δg_Z^1 parameter using a maximum likelihood fit to the two dimension P_{Z}^T vs. P_{lW}^T distribution is

$$-0.0064_{\mathrm{stat.}},\quad -0.0058_{\mathrm{syst.}} < \Delta g_Z^1 < +0.010_{\mathrm{stat.}},\quad +0.0058_{\mathrm{syst.}} \tag{17}$$

which gives

$$-0.0086 < \Delta g_Z^1 < 0.011 \tag{18}$$

when the statistical and systematic contributions are added in quadrature.

We emphasise that we have used a pessimistic treatment of the systematic errors in this study.

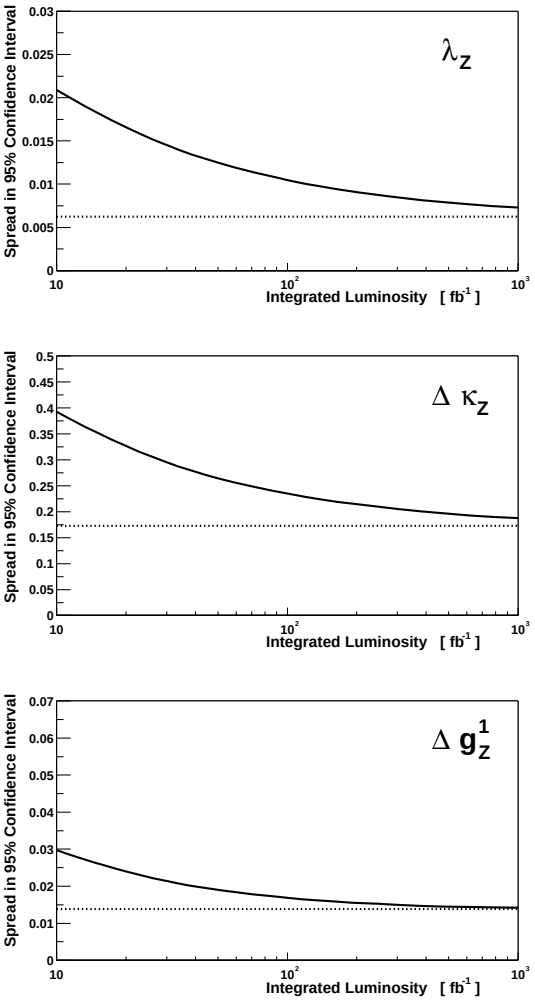

FIG. 6: The 95% confidence intervals (solid lines) are shown as a function of integrated luminosity for WZ production at the LHC. The dotted lines indicate the magnitude of the systematic contributions, which are added in quadrature to the 95% statistical confidence limits to obtain the total confidence intervals (shown as solid lines).

D. Limits as a Function of Integrated Luminosity

In Figure 6, the spread in the confidence intervals for the anomalous TGC parameters (extracted from the P_Z^T distribution) are shown as a function of integrated luminosity. The ATLAS experiment is expected to collect about 30 fb^{-1} at low luminosity and 300 fb^{-1} at high luminosity. These results should be interpreted with caution since they have been constructed by simply scaling the histograms which were constructed to study the sensitivity of the ATLAS experiment for low luminosity LHC running and changes in effects like pile-up have not been accounted for.

For the $\Delta\kappa_Z$ and λ_γ parameters, statistics dominate the confidence intervals up to about $\mathcal{L} = 100$ fb^{-1}. These parameters are particularly sensitive to the modelling of the proton structure with the p.d.f.'s. A careful understanding and evaluation of these effects will be important for measurements of the $\Delta\kappa_Z$ and λ_γ parameters at the LHC using data samples in excess of 100 fb^{-1}.

The systematics and statistics provide contributions of similar size to the confidence intervals for the Δg_Z^1 parameter at 30 fb^{-1}. Very little can be gained for this parameter by increasing the integrated luminosity, unless the systematics can be controlled at a level beyond what has

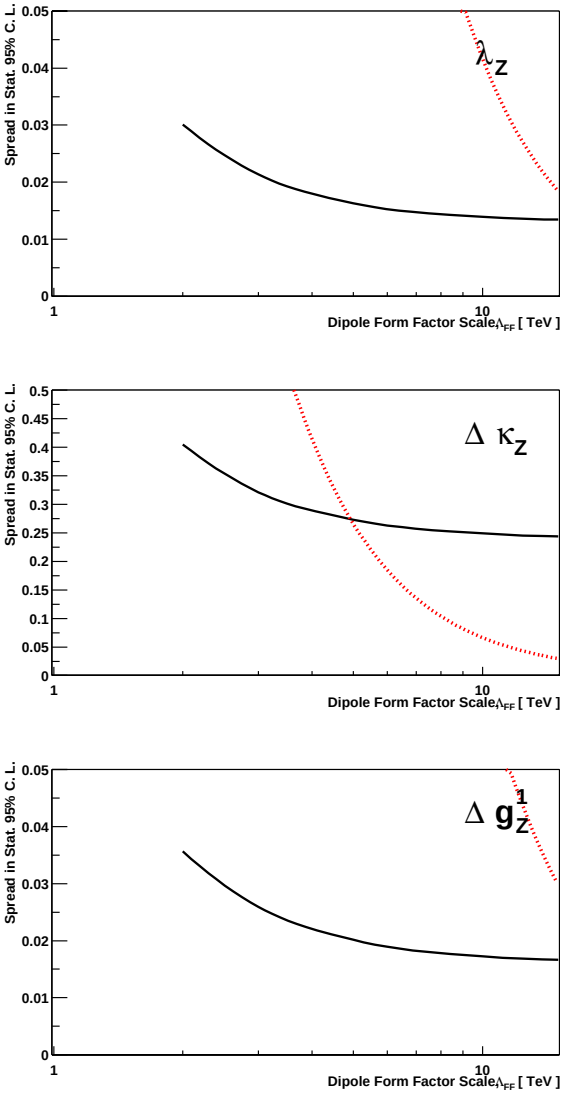

FIG. 7: The spread in statistical 95% confidence intervals (solid lines) are shown as a function of the dipole form factor scale assumption $\Lambda_{\rm FF}$ for WZ production at the LHC. The dotted lines indicate the approximate Born level unitarity limits [10]. The region above the solid line is excluded by the experiment, while the region to the right of the dotted line is excluded by unitarity.

been assumed for this study (recall that the systematics considered here are pessimistic).

E. Limits as a Function of Form Factor Scale and Mass Scale

For the results presented thus far, the anomalous TGC's have been assumed constant (i.e. $\Lambda_{\rm FF} = \infty$), which would be in violation of unitarity at high energy scales.

The spread in the statistical 95% confidence limits are presented in Figure 7 as a function of form factor scale $\Lambda_{\rm FF}$, assuming the dipole (n=2) form factor expression (which is the conventional form factor assumption) of Eq. 4. The limits turn asymptotic at about $\Lambda_{\rm FF} = 5$ to 10 TeV. This means that the constant anomalous TGC's used in this study provide equivalent results as would be obtained with a dipole form factor down to scales of about 5 TeV.

Unitarity provides stricter bounds on the $\Delta\kappa_Z$ parameter for $\Lambda_{\rm FF}$ >5 TeV than will be obtained with 30 fb^{-1} at the LHC. This means that if one wishes to have limits which are strictly within the unitarity allowed region, a form factor scale smaller than 5 TeV would need

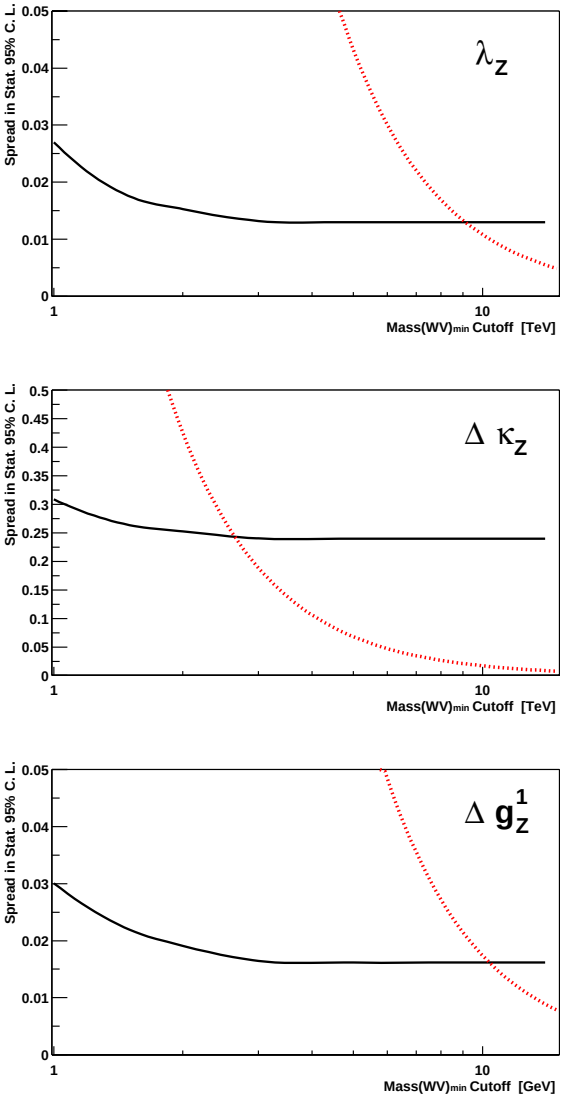

FIG. 8: The spread in statistical 95% confidence intervals (solid lines) are shown for WZ production as a function the diboson mass cutoff, which is used as a selection criteria for events included in the analysis. The dotted lines indicate the approximate Born level unitarity limits from Eq. 3. An integrated luminosity of 30 fb^{-1} at the LHC has been assumed. The region above the solid line is excluded by the experiment, while the region to the right of the dotted line is excluded by unitarity.

to be employed.

We have argued in Section II that the introduction of a form factor assumption into the model is unnecessary, if instead the limits are reported as a function of a diboson invariant mass cutoff applied to the data. This treatment ensures unitarity, without the need to introduce new parameters to parametrise the form factor behaviour.

In Figure 8 the limits are presented as a function of a diboson mass cutoff (the minimum of the two reconstructed mass solutions is used). For example, the limits at Mass$(WZ)_{\rm min} = 2$ TeV use only the data for which the reconstructed minimum mass solution is less than 2 TeV. As for the dipole form factor scale, an asymptotic limit is reached. This time the limit is at about 3 TeV. The unitarity limit is superimposed on the plots as a dotted line (here the unitarity limits of Eq. 3 are the relevant ones). The region above the solid line is excluded by the experiment, while the region to the right of the dotted line is excluded by unitarity.

This strategy allows for the presentation of limits without introducing arbitrary choices for the energy dependent form factor parametrisation. It shows the ultimate reach of the experiment, while allowing the interpretation of the results at any mass scale. Further, if an

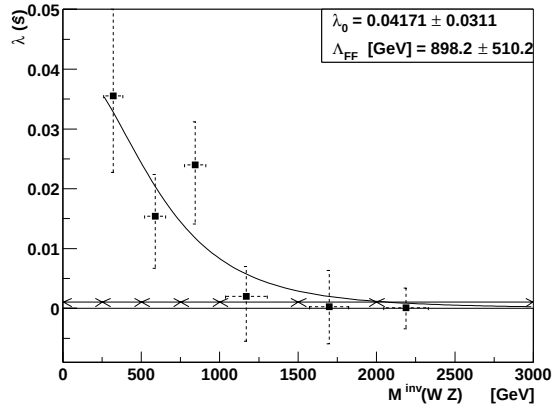

FIG. 9: Measurement of the λ_Z parameter as a function of energy is demonstrated using 30 fb^{-1} integrated luminosity for LHC WZ production. The 'mock' ATLAS data has been generated with λ_{Z0}=0.04 using a dipole form factor of scale $\Lambda_{\rm FF}$ = 1500 GeV. The solid line is a fit to $\Lambda_{\rm FF}$ and the bare coupling λ_{Z0} assuming the dipole form factor. The arrows along the x-axis indicate the diboson mass bin widths.

anomalous coupling 'turns on' or 'turns off' at some mass scale, that would be reflected in the limits.

In the scenario where anomalous TGC measurements at LHC are inconsistent with the Standard Model, it would be preferable to measure the energy dependence of the anomalous TGC parameters directly, rather than assuming some energy dependence in the model. The feasibility of such a measurement at hadron colliders has been suggested in Ref. [30] and demonstrated in Refs. [4, 31]. In Figure 9, we repeat the study which has been presented for $W\gamma$ production in Ref. [1], and demonstrate this type of analysis for the λ_Z parameter.

A large data sample of diboson events will be necessary to perform such a measurement, because the data needs to be separated out into bins of diboson mass. For Figure 9, 'mock' ATLAS data has been generated with bare coupling $\lambda_{Z0} = 0.04$ and a dipole (n=2) form factor with $\Lambda_{\rm FF} = 1500$ GeV. This 'mock data' is then compared to reference histograms of the bare coupling λ_{Z0} (i.e. the reference histograms do not use a form factor) for each of the diboson mass bins. The events have been separated out into diboson mass bins ranging from 250 GeV to 3000 GeV with variable width, to ensure adequate statistics in each bin. The behaviour of the couplings as a function of energy is clearly visible. A fit to the dipole form factor function is also indicated with a solid line. The parameters which were used to generate the 'mock' data are reproduced within the precision of the fit.

As compared to the energy dependent measurement of the λ_γ parameter presented in Ref. [1], the measurement of the λ_Z parameter energy dependence is slightly more difficult, because of the lower WZ event rate. Measurements of the λ_Z parameter energy dependence is feasible with about 30 fb^{-1} of LHC data. Measurements of the $\Delta\kappa_Z$ and Δg_Z^1 parameters require more data, and will likely not be feasible at the LHC with precisions that have not already been excluded by LEP and Tevatron data.

VI. CONCLUSIONS

The prospects for measuring the WWZ triple gauge-boson coupling (TGC) using the electron and muon decay channels of $pp \to WZ$ production at the LHC have been assessed in the context of the ATLAS experiment. The analysis assumes low luminosity (10^{33}cm^{-2}s^{-1}) LHC conditions and an integrated luminosity of 30 fb^{-1}.

The signal to background ratio after applying kinematic cuts is about 20, and the modeling of the backgrounds will not be an important systematic effect for these measurements.

In the scenario where the anomalous TGC parameters are consistent with the Standard Model, confidence limits can be extracted using a maximum likelihood fit to one or two dimension distributions. The one dimension transverse momentum of the Z-boson distribution ($P_{\rm Z}^T$) and the two dimension transverse momentum of the Z-boson versus transverse momentum of the charged lepton from the W-decay ($P_{\rm Z}^T$ vs. $P_{\rm l_W}^T$) distribution provide the most stringent confidence intervals. These distributions show the smallest sensitivity to systematic biases. The expected 95% confidence intervals for the WWZ vertex anomalous couplings are

$$\begin{array}{cccccc}
-0.0065_{\rm stat.}, & -0.0032_{\rm syst.} & < \lambda_Z < & +0.0066_{\rm stat.}, & +0.0031_{\rm syst.} \\
-0.10_{\rm stat.}, & -0.024_{\rm syst.} & < \Delta\kappa_Z < & +0.12_{\rm stat.}, & +0.024_{\rm syst.} \\
-0.0064_{\rm stat.}, & -0.0058_{\rm syst.} & < \Delta g_Z^1 < & +0.010_{\rm stat.}, & +0.0058_{\rm syst.}
\end{array}$$

using 30 fb^{-1} (about 3 years) of low luminosity LHC data.

For the λ_Z and $\Delta\kappa_Z$ parameters, the confidence intervals will be dominated by statistics for integrated luminosities beyond 100 fb^{-1}. Our ability to model the proton structure with the parton density functions is the dominant systematic. Systematic effects are more important for measurements of the Δg_Z^1 parameter.

Dipole form factors have been the conventional means of guaranteeing unitarity in the TGC Lagrangian. The parametrization of the form factors is arbitrary, and introduces unnecessary dependence on the parametrization choice into the experimental results. Though the confidence intervals as a function of a dipole form factor parametrization have been included in this study, it has been argued here that it is preferable to report the limits as a function of a diboson invariant mass cutoff which is applied to the data. The LHC data will directly probe diboson invariant mass scales up to about 3 TeV, which is the scale at which the limits as a function of the mass cutoff turn asymptotic. Since unitarity is violated only for diboson mass cutoffs above 3 TeV (or in the $\Delta\kappa_Z$ case, at about 3 TeV), the limits reported here are unitarity safe, and are presented without any cutoff or form factor.

Acknowledgements

We have benefited from discussions with Jorgen Beck Hansen and Samira Hassani. We are grateful to Ulrich Baur for informative correspondence, comments, and discussions. This work has been supported by the Natural Sciences and Engineering Research Council of Canada.

---

[1] M. Dobbs and M. Lefebvre, "Prospects for Probing the Three Gauge-boson Couplings in W + Photon Production at the LHC", ATLAS Internal Note, ATL-COM-PHYS-2002-019, 2002.

[2] D. Fouchez, "Gauge boson pairs production study with Atlas", ATLAS Internal Note PHYS-NO-060, 24 November, 1994.

[3] J.B. Hansen, "Triple Gauge-boson Couplings in Boson Pair Production", presented at the ATLAS Physics Week in Grenoble April 1998.

[4] S. Hassani, "Prospects for Measuring Neutral Gauge Boson Couplings in ZZ Production with the ATLAS Detector", ATLAS Internal Communication ATL-COM-PHYS-2002-012, 2002;
S. Hassani, "Prospects for Measuring Neutral Gauge Boson Couplings in $Z\gamma$ Production with the ATLAS Detector", ATLAS Internal Communication ATL-COM-PHYS-2002-013, 2002.

[5] K. Hagiwara, R. D. Peccei, D. Zeppenfeld and K. Hikasa, "Probing the Weak Boson Sector in $e^+e^- \to W^+W^-$," Nuclear Physics B **282**, 253 (1987).

[6] D. Zeppenfeld and S. Willenbrock, "Probing the Three Vector-Boson Vertex at Hadron Colliders," Physical Review D **37**, 1775 (1988).

[7] U. Baur and D. Zeppenfeld, "Probing the $WW\gamma$ Vertex At Future Hadron Colliders," Nuclear Physics B **308**, 127 (1988).

[8] G. Gounaris, J.L. Kneur, D. Zeppenfeld, Z. Ajaltouni, A. Arhrib, G. Bella, F. Berends, M. Bilenkii, A. Blondel, J. Busenitz, D. Charlton, D. Choudhury, P. Clarke, J.E. Conboy, M. Diehl, D. Fassouliotis, J.M. Frere, C. Georgiopoulos, M. Gibbs, M. Grunewald, J.B. Hansen, C. Hartmann, B.N. Jin, J. Jousset, J. Kalinowski, M. Kocian, A. Lahanas, J. Layssac, E. Lieb, C. Markou, C. Matteuzzi, P. Mattig, J.M. Moreno, G. Moultaka, A. Nippe, J. Orloff, C.G. Papadopoulos, J. Paschalis, C. Petridou, H. Phillips, F. Podlyski, M. Pohl, F.M. Renard, J.M. Rossignol, R. Rylko, R.L. Sekulin, A. van Sighem, E. Simopoulou, A. Skillman, V. Spanos, A. tonazzo, M. Tytgat, S. Tzamarias, C. Verzegnassi, N.D. Vlachos, E. Zevgolatakos, "Triple Gauge Boson Couplings", in **Physics at LEP2**, vol. 1 525-576 [hep-ph/9601233], 1996.

[9] K. Hagiwara, S. Ishihara, R. Szalapski and D. Zeppenfeld, "Low-energy effects of new interactions in the electroweak boson sector," Physical Review D **48**, 2182 (1993).

[10] U. Baur, D. Zeppenfeld, "Unitarity Constraints on the Electroweak Three Vector Boson Vertices," Physics Letters B **201**, 383 (1988).

[11] U. Baur, T. Han and J. Ohnemus, "WZ production at hadron colliders: Effects of nonstandard WWZ couplings and QCD corrections," Physical Review D **51**, 3381 (1995) [hep-ph/9410266].

[12] K. O. Mikaelian, "Photoproduction of Charged Intermediate Vector Bosons," Phys. Rev. **D 17**, 750 (1978);
K. O. Mikaelian, M. A. Samuel and D. Sahdev, "The Magnetic Moment of Weak Bosons Produced in pp and $p\bar{p}$ Collisions," Phys. Rev. Lett. **43**, 746 (1979);
R. W. Brown, D. Sahdev and K. O. Mikaelian, "$W^{\pm}Z^0$ and $W^{\pm}\gamma$ Pair Production in νe, pp, and $p\bar{p}$ Collisions," Phys. Rev. **D 20**, 1164 (1979);
T. R. Grose and K. O. Mikaelian, "W and Z^0 Decays Into Quarks Plus a Photon or a Gluon," Phys. Rev. **D 23**, 123 (1981);
S. J. Brodsky and R. W. Brown, "Zeros In Amplitudes: Gauge Theory and Radiation Interference," Phys. Rev. Lett. **49**, 966 (1982);
M. A. Samuel, "Amplitude Zeros," Phys. Rev. **D 27**, 2724 (1983);
R. W. Brown, K. L. Kowalski and S. J. Brodsky, "Classical Radiation Zeros in Gauge Theory Amplitudes," Phys. Rev. **D 28**, 624 (1983);
R. W. Brown and K. L. Kowalski, "Classical Radiation Zeros Addendum: Spin Dependent Null Zone," Phys. Rev. **D 29**, 2095 (1984).

[13] U. Baur, T. Han and J. Ohnemus, "Amplitude zeros in $W^{\pm}Z$ production," Physical Review Letters **72**, 3941 (1994) [hep-ph/9403248].

[14] The LEP Collaborations Aleph, Delphi, L3, OPAL and the Electroweak Working Group, "A combination of preliminary electroweak measurements and constraints on the standard model," hep-ex/0103048, February 2001.

[15] H. L. Lai *et al.*, "Improved parton distributions from global analysis of recent deep inelastic scattering and inclusive jet data," Physical Review D **55**, 1280 (1997) [hep-ph/9606399].

[16] R. K. Ellis, W. J. Stirling and B. R. Webber, "QCD and Collider Physics," Cambridge Monographs in Particle Physics, Nuclear Physics and Cosmology **8**, 1 (1996).

[17] T. Sjöstrand, P. Eden, C. Friberg, L. Lönnblad, G. Miu, S. Mrenna and E. Norrbin, "High-energy-physics event generation with PYTHIA 6.1," Computer Physics Communications **135**, 238 (2001) [hep-ph/0010017].

[18] E. Richter-Was, D. Froidevaux, and L. Poggioli, "ATLFAST 2.0 a fast simulation package for ATLAS", ATLAS Internal Communication ATL-PHYS-98-131, 1998.

[19] The ATLAS Collaboration, *ATLAS Detector and Physics Performance Technical Design Report*, CERN/LHCC/99-14 and CERN/LHCC/99-15, 25 May 1999.

[20] P. Pralavorio, "Electron/Jet Separation with the ATLAS Detector", ATLAS Internal Note ATL-PHYS-99-015, 1999.

[21] The ATLAS Collaboration, *ATLAS Technical Proposal*, CERN/LHCC/94-43, 15 December 1994.

[22] E. Maina and S. Moretti, "Z^0, γ production in association with top quark pairs," Phys. Lett. B

286, 370 (1992).
[23] H. L. Lai *et al.*, "Global QCD analysis and the CTEQ parton distributions," Physical Review D **51**, 4763 (1995) [hep-ph/9410404].
[24] M. Diehl and O. Nachtmann, "Optimal observables for the measurement of three gauge boson couplings in $e^+e^- \to W^+W^-$," Zeitschrift für Physik C **62**, 397 (1994).
[25] A. Heister *et al.* [ALEPH Collaboration], "Measurement of triple gauge boson couplings at LEP energies up to 189 GeV," European Physical Journal C **21**, 423 (2001) [hep-ex/0104034].
[26] G. Abbiendi *et al.* [OPAL Collaboration], "Measurement of triple gauge boson couplings from W^+W^- production at LEP energies up to 189 GeV," European Physical Journal C **19**, 1 (2001) [hep-ex/0009022].
[27] M. Acciarri *et al.* [L3 Collaboration], "Measurement of triple-gauge-boson couplings of the W boson at LEP," Physics Letters B **467**, 171 (1999) [hep-ex/9910008].
[28] P. Abreu *et al.* [DELPHI Collaboration], "Measurements of the trilinear gauge boson couplings WWV ($V = \gamma, Z$) in e^+e^- collisions at 183 GeV," Physics Letters B **459**, 382 (1999).
[29] L. Dixon, Z. Kunszt and A. Signer, "Vector boson pair production in hadronic collisions at $O(\alpha_S)$: Lepton correlations and anomalous couplings," Physical Review D **60**, 114037 (1999) [hep-ph/9907305].
[30] G. J. Gounaris, J. Layssac and F. M. Renard, "Signatures of the anomalous $Z\gamma$ and ZZ production at the lepton and hadron colliders," Physical Review D **61**, 073013 (2000) [hep-ph/9910395].
[31] M. Dobbs, "Unitarity Limits and Form Factors", contribution to S. Haywood *et al.* "Electroweak Physics", in the *Proceedings of the Standard Model Physics (and more) at the LHC Workshop*, Geneva, 1999, CERN-TH-2000-102 [hep-ph/0003275].

APPENDIX

Effect of Isolation Criteria on $Z \to e^+e^-$ Decays

Reconstructed electron, muon, and photon candidates in `ATLfast` are required to satisfy isolation criteria. This means that their signatures in the detector are required to be well separated from those of other particles and maximises the probability that the energy deposition in the detector has been properly assigned to the correct particle candidate.

The isolation criteria which have been used for this study are the default criteria implemented in the `ATLfast` detector simulation. The candidate particle is required to be separated from the centre of electromagnetic or hadronic calorimeter clusters[2] by a distance in the pseudo-rapidity and azimuthal plane of at least $\Delta R = \sqrt{\Delta\phi^2 + \Delta\eta^2}$=0.4. In addition, the amount of electromagnetic and hadronic calorimeter transverse energy lying within a cone of ΔR=0.2 from the particle candidate is required to be no more than 10 GeV.

These criteria are particularly relevant for the reconstruction of the Z-boson in WZ production. When the Z decays to e^+e^-, the reconstructed electron must be separated from the reconstructed positron by at least ΔR =0.4, whereas the muons in the $Z \to \mu^+\mu^-$ decay channel need not be separated at all (since they deposit essentially no electromagnetic or hadronic energy). For very high transverse momentum $Z \to e^+e^-$ decays, this can result in a substantial loss of efficiency, since the boost of the Z-boson can cause the decay products to be highly collimated. This is demonstrated in Figure 10, for the special case of Z^0-bosons travelling transverse to the beam (i.e. $P_Z^L = 0$). The ΔR separation of the electron from the positron is shown (top) as a function of the Z^0 transverse momentum and $\cos\theta^\star_{Z\to ee}$, where $\theta^\star_{Z\to ee}$ is the production angle of the electron in the Z rest frame with respect to the beam direction. In

[2] Calorimeter clusters are defined using a cone algorithm with ΔR =0.4.

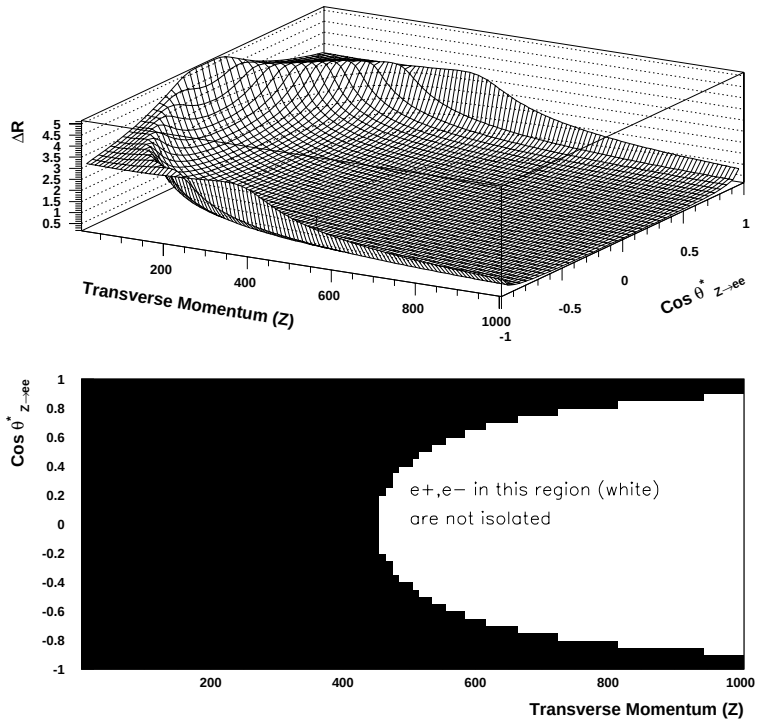

FIG. 10: The ΔR separation of the electron from the positron is shown (top) for $Z^0 \to e^+e^-$ decays with the Z^0-boson travelling transverse to the beam as a function of the Z^0 transverse momentum and $\cos\theta^{\star}_{Z\to ee}$. The $Z^0 \to e^+e^-$ decays which would fail the isolation criteria are shown (bottom) in white as a function of the Z^0 transverse momentum and $\cos\theta^{\star}_{Z\to ee}$.

Figure 10 (bottom), the $Z^0 \to e^+e^-$ decays which would fail the isolation criteria are shown in white as a function of the Z^0 transverse momentum and $\cos\theta^{\star}_{Z\to ee}$.

For a cone size ΔR =0.4, $Z^0 \to e^+e^-$ decays begin to fail the isolation criteria above $P_{\rm Z}^T = 450$ GeV, and so does not affect this analysis, since fewer than a single event is expected in that region for an integrated luminosity of 30 fb^{-1}. However, for high luminosity running at the LHC, this can start to be a significant effect, particularly since this is precisely the regime where the effects of anomalous TGC's are largest. TGC analyses which are applied to several years of high luminosity LHC data would have to use modified isolation criteria for electrons to account for this effect.

In order to evaluate the size of this effect for a physical process, we generate $pp \to Z\gamma \to e^+e^-\gamma$ events with `PYTHIA` 6.136, and turn off all electromagnetic and QCD parton showering, such that the final state contains only the electron, positron, and photon. The events are passed to `ATLfast`, and the average efficiency as a function of Z^0 transverse momentum is shown in Figure 11. As expected, the efficiency (fraction of electron positron pairs which satisfy the isolation) drops substantially above $P_{\rm Z}^T = 450$ GeV.

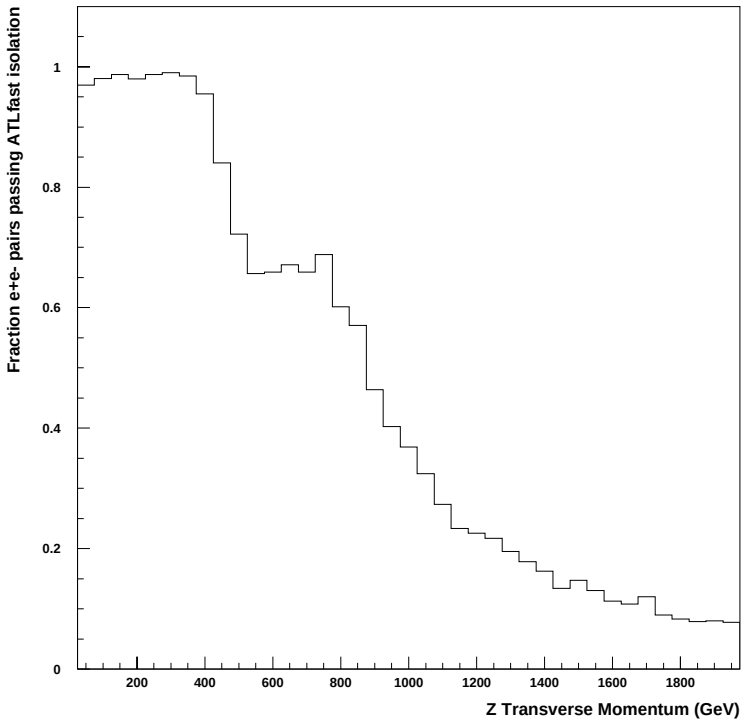

FIG. 11: The fraction of e^+e^- pairs which satisfy the `ATLfast` isolation criteria in $pp \to Z\gamma \to e^+e^-\gamma$ production at the LHC as a function of the Z^0 transverse momentum is shown.